



Article

Characterization of Burn Eschar Pericytes

Alexander Evdokiou¹, Onur Kanisicak², Stephanie Gierek¹, Amanda Barry¹ , Malina J. Ivey², Xiang Zhang³ , Richard J. Bodnar⁴ and Latha Satish^{1,2,*}

¹ Shriners Hospitals for Children, Research Department, Cincinnati, OH 45229, USA; evdokioua@gmail.com (A.E.); sjgierek@gmail.com (S.G.); ambarry@shrinenet.org (A.B.)

² Department of Pathology and Laboratory Medicine, University of Cincinnati, Cincinnati, OH 45267-0529, USA; kanisior@ucmail.uc.edu (O.K.); malina.ivey@uc.edu (M.J.I.)

³ Genomics, Epigenomics and Sequencing Core, University of Cincinnati, Cincinnati, OH 45267, USA; zhanx5@ucmail.uc.edu

⁴ Veterans Affairs Medical Center, University Dr. C, Pittsburgh, PA 15240, USA; Richard.bodnar@va.gov

* Correspondence: lsatish@shrinenet.org or satishla@ucmail.uc.edu; Tel.: +1-513-872-6278

Received: 10 February 2020; Accepted: 19 February 2020; Published: 24 February 2020



Abstract: Pericytes are cells that reside adjacent to microvasculature and regulate vascular function. Pericytes gained great interest in the field of wound healing and regenerative medicine due to their multipotential fate and ability to enhance angiogenesis. In burn wounds, scarring and scar contractures are the major pathologic feature and cause loss of mobility. The present study investigated the influence of burn wound environment on pericytes during wound healing. Pericytes isolated from normal skin and tangentially excised burn eschar tissues were analyzed for differences in gene and protein expression using RNA-seq., immunocytochemistry, and ELISA analyses. RNA-seq identified 443 differentially expressed genes between normal- and burn eschar-derived pericytes. Whereas, comparing normal skin pericytes to normal skin fibroblasts identified 1021 distinct genes and comparing burn eschar pericytes to normal skin fibroblasts identified 2449 differential genes. Altogether, forkhead box E1 (FOXE1), a transcription factor, was identified as a unique marker for skin pericytes. Interestingly, FOXE1 levels were significantly elevated in burn eschar pericytes compared to normal. Additionally, burn wound pericytes showed increased expression of profibrotic genes periostin, fibronectin, and endosialin and a gain in contractile function, suggesting a contribution to scarring and fibrosis. Our findings suggest that the burn wound environment promotes pericytes to differentiate into a myofibroblast-like phenotype promoting scar formation and fibrosis.

Keywords: pericyte; periostin; FoxE1; IL-6; IL-8; MYD88; TGF- β ; endosialin; burns and stem cells

1. Introduction

Severe burn injury results in devastating scarring and contractures. Several cell populations, including inflammatory cells, fibroblasts, and keratinocytes, play a crucial role in coordinating the wound healing outcome [1,2]. Recently, pericytes (PCs), a mesenchymal stem cell-like population, have been reported to contribute to liver [3], lung [4], kidney [5], and skin fibrosis [6]. However, PCs role in burn wound healing is still yet to be deciphered. Burn wound environment is an atypical niche compared to incisional or excisional skin injury with excessive inflammation and a prolonged influx of inflammatory cells lasting for several days [7]. The goal of the present study is to capture the changes that might occur to pericytes in burn wounds and their role in wound healing including scarring and contractures.

PCs are perivascular cells with long surface processes that encircle microvascular endothelial cells (ECs) and provide important structural integrity to the vessel wall through direct and indirect signaling mechanisms. [8,9]. PCs promote activation of latent transforming growth factor (TGF)- β

inducing EC proliferation and differentiation through T β R/ALK/Smad pathways [10], regulate vessel remodeling through the IP-10/CXCR3 signaling pathway [11,12] and maturation through the expression of Ang 1 [13]. In addition, PCs can regulate immune response through the secretion of cytokines and chemokines [14,15].

Due to limited cell-specific markers, identification and characterization of PCs in burn wound healing have been unreliable. Some of the commonly used markers to identify PCs are neuron-gial 2 (NG2), platelet-derived growth factor receptor beta (PDGFR- β), CD146, alpha-smooth muscle actin (α -SMA), and regulator of G protein signaling 5 (RGS-5) [16]. Mesenchymal stem cell (MSC) markers CD44, CD73, CD90, and CD105 have also been used to identify pericytes [16]. During vessel remodeling however, the expression of CD146 and PDGFR- seem to be ubiquitous, and RGS-5 is upregulated on activated PCs [17]. Pericytes have been observed to be multipotent, thus have been identified as a MSC progenitor [16,18,19]. It is well established that MSC site of origin influences their functional properties, pericyte function seem to also be influenced by their origin and surroundings [20]. It has been postulated that pericyte function may be different in fetal/young tissue compared to adult tissue and not all pericytes are MSCs [21]. Therefore, understanding the signals that regulate pericyte function will provide a better understanding of the role pericytes play in tissue regeneration.

Recent studies have shown that pericytes play a role in wound healing [22–25], but their significance is not well understood. In wound healing, pericytes contribute to angiogenesis (EC migration and proliferation, wound stabilization, and regression) [12,26,27], inflammation (neutrophil and macrophage extravasation, and T cell activation) [28–31], re-epithelialization [32], tissue regeneration [29], and fibrosis [32,33]. Our understanding of the involvement of PCs in these functions is still in its infancy. The inflammatory phase of wound healing plays a critical role in the healing process. Any perturbations in the process can lead to delayed healing, fibrosis, or ulcer formation. In this phase, PCs have been observed to have multiple functions. They help to initiate angiogenesis by retracting from the microvessels, promoting dissociation of cell-cell interaction, and promoting EC migration and proliferation [25]. PCs have also been found to be directly involved in the extravasation of neutrophils and macrophages [34]. In addition, matrix deposition in wound healing is essential for wound closure and strength of the skin. Fibroblasts are the principal cell involved in matrix deposition and organization. The dysregulation of fibroblasts promotes excessive collagen production which can lead to fibrosis. Recent studies have shown that PCs have the ability to secrete collagen and contribute to fibrosis [35–37]. In a study by Birbrair et al., two distinct PC sub-types were identified, where type 1 PCs secrete collagen and promote fibrosis [35]. These studies suggest that dysregulation of pericytes can play a significant role in fibrosis. Here we evaluated the gene expression of pericytes from burn eschar. We are the first to identify the expression of forkhead box E1 (FOXE1) in pericytes. We also show that pericytes from burn eschar have a high expression of the pro-fibrotic genes fibronectin, myeloid differentiation factor 88 (MyD88), periostin and endosialin, and the pro-inflammatory cytokines IL-6 and IL-8. Characterization of pericytes from burn eschar suggest that the burn wound environment potentiates pericytes to a myofibroblast-like phenotype (collagen producing cell), which can lead to or promote fibrosis.

2. Experimental Section

2.1. Discarded Human Skin Tissues

Tangentially excised burn eschar was obtained from the routine debridement procedure, which occurs within a week after burn injury. Healthy normal skin was obtained as excess during elective plastic surgery procedures. All tissue was obtained from patients treated at Shriners Hospitals for Children-Cincinnati or the University of Cincinnati Medical Center, Cincinnati, OH. The University of Cincinnati Institutional Review Board determined that this does not constitute human subjects research and is exempt from requirements for informed consent according to 45CFR46.101 (b) (4). Patient information was anonymized, and samples were de-identified prior to analysis. Strain numbers were

used to enable de-identification and were assigned sequentially to all the samples collected by the laboratory. For the current study, experiments were performed using burn eschar tissues collected from six different patients, and excess discarded normal skin from six different patients were used. Table 1 provides demographic information.

Table 1. Demographic information on burn eschar and normal skin tissues used for pericytes isolation.

Strain no.	Age	Race	Sex	Type of Burns	Body Site Debridement/Excision/Surgical Procedure
Burn Eschar					
Burn 8	11 yrs	Other	Female	Scald	Bilateral Lower Legs
Burn 18	2 months	Black/Non-Hispanic	Female	Contact	Left thigh, Foot and Leg
Burn 20	2 yrs	Hispanic	Male	Scald	Anterior Trunk
Burn 21	16 months	White/Non-Hispanic	Female	Scald	Scalp
Burn 22	9 yrs	White/Non-Hispanic	Male	Female	Left Flank, Left Leg and Left Axilla
Burn 23	9 yrs	White/Non-Hispanic	Male	Female	Chest and Abdomen
Normal Skin					
Normal Skin 1	16 yrs	White	Female	N/A	Breast Reduction
Normal Skin 4	14 months	White	Female	N/A	Excess Tissue From Right Thigh Was Used After Using for a Split Skin Thickness Graft
Normal Skin 8	16 yrs	Black/Non-Hispanic	Female	N/A	Breast Reduction
Normal Skin 9	13 yrs	White	Female	N/A	Breast Reduction
Normal Skin 11	16 yrs	African American	Female	N/A	Breast Reduction
Normal Skin 13	18 yrs	Biracial White/Black	Female	N/A	Breast Reduction

2.2. Pericytes and Fibroblasts Cultures

Primary cultures of pericytes were isolated from discarded normal and burn eschar skin without the use of enzymatic digestion. Skin samples were placed into Pericyte Medium (Zenbio Inc. Research Triangle, NC, USA), cut into thin strips, and scrapped using forceps. Following a 48 h incubation period, the dish was washed twice with 1× PBS (Thermo Fisher Scientific, Waltham, MA, USA), and the media was changed. The cells were allowed to expand to 80% confluence and then frozen for future analysis. Primary cultures of fibroblasts established using discarded normal skin was used as described in detail elsewhere [38].

2.3. Flow Cytometry

A Beckman Coulter MoFlo Astrios EQ flow cytometer (Beckman Coulter, Indianapolis, IN, USA) was used to identify and enrich the pericyte population from the cells isolated from the eschar skin using the following panel of antibodies: positive PE conjugated anti-CD146 (BD Biosciences, San Jose, CA, USA), positive APC conjugated CD-105 (BioLegend, San Diego, CA, USA), positive Brilliant Violet 421 conjugated anti-CD73 (BioLegend), negative SuperBright 600 conjugated anti-CD56 (Thermo Fisher Scientific, Waltham, MA, USA), negative BrilliantBlue 515 conjugated anti-CD45 (BD Biosciences), and negative PerCP-eFluor 710 conjugated anti-CD34 (Thermo Fisher Scientific). Sorted pericytes were used for each experiment. A BD LSRII flow cytometer (BD Biosciences) was used

to phenotype the expression of surface markers on pericytes and fibroblasts using PE conjugated anti-CD146 (BD Biosciences), APC conjugated CD-105 (BioLegend), Brilliant Violet 421 conjugated anti-CD73 (BioLegend), SuperBright 600 conjugated anti-CD56 (Thermo Fisher Scientific), BrilliantBlue 515 conjugated anti-CD45 (BD Biosciences), and PerCP-eFluor 710 conjugated anti-CD34 (Thermo Fisher Scientific). This panel was specifically chosen using the application Fluoro Finder to minimize spectral overlap. 1×10^6 cells were placed in individual polystyrene tubes, washed twice with $1 \times$ PBS, fixed using 4% paraformaldehyde (Affymetrix; Thermo Fisher Scientific) for 10 min, washed twice more, then stained for marker expression. During analysis, 10,000 events per antibody of interest were analyzed, and data are presented as % positive of the gated population \pm SEM.

2.4. Immunocytochemistry & Immunohistochemistry

Immunocytochemistry: Pericytes and fibroblasts were grown to 85% confluence on 8-well chamber polystyrene slides (Falcon; Thermo Fisher Scientific) at a concentration of 10^4 cells per chamber. Cells were fixed with 4% paraformaldehyde and washed twice with $1 \times$ PBS. Following fixation, cells were stained with anti-CD146 (1:250; Abcam, Cambridge, MA, USA), S100A4 (1:250; Abcam), NG2 (1:200 Sigma-Aldrich, St. Louis, MO, USA), myosin smooth muscle heavy chain (MHY11, 1:200; Invitrogen, Thermo Fisher Scientific; MA511971), Calponin-1 (1:200; Invitrogen MA511620), Transgelin/ smooth muscle 22 (SM22) (1:200; Proteintech 104931AP) and incubated overnight at 4 °C. Slides were then washed twice with $1 \times$ PBS, stained with DAPI mounting medium (Vector Laboratories Inc, Burlingame, CA, USA), and imaged using Eclipse 90i microscope equipped with a Ds-Ri1 Digital Microscope Camera (Nikon Instruments Inc., Melville, NY, USA).

Immunohistochemistry: Discarded normal skin and burn eschar tissue were embedded frozen for cryosectioning using OCT Compound (Fisher HealthCare, Pittsburgh, PA, USA). Immunohistochemistry was performed on cryosections prepared by Shriners Hospitals for Children-Cincinnati Histology Special Shared Facility. Sections were incubated with primary antibody for CD-146 (cat.no. ab 78451; 1:200; Abcam) and periostin (cat. no: ab 215199; 1:200; Abcam) overnight at 4 °C. Secondary antibodies against CD-146 (ab 150117; Abcam; 1:400) and periostin (A21207; Thermo Fisher Scientific; 1:400) was incubated for 1 h at room temperature. Vectashield Antifade Mounting Medium with DAPI (4'-diamidino-2-phenylindole, Cat.no. H-1200, Vector Laboratories) was used to mount coverslips and counterstain nuclei. Sections were viewed and photographed with an Eclipse 90i microscope equipped with a Ds-Ri1 Digital Microscope Camera (Nikon Instruments Inc.). Z-stacking was used to improve the depth of the field of digital images. All images for a given antibody were collected using identical settings for each tissue section.

2.5. RNA-seq Analysis and Quantitative Real-Time RT-PCR (RT-qPCR)

Total RNA was isolated from normal skin pericytes, burn eschar pericytes, and normal skin fibroblasts using RNeasy Mini Kit (Qiagen Inc, Valencia, CA, USA) following the manufacturer's instructions. The quantity and quality of RNA were determined by measuring the OD 260/280 ratio using an ND-100 spectrophotometer (Nanodrop Technologies Inc., Wilmington, DE, USA) and by capillary electrophoresis using an Agilent 2100 BioAnalyzer (Santa Clara, CA, USA). The RNA with a RIN value >7 was used for RNA-seq analysis and RT-qPCR assays. RNA-seq analysis was conducted in the Genomics, Epigenomics, and Sequencing Core at the University of Cincinnati. The polyA RNA was isolated from ~200 ng total RNA using NEBNext Poly(A) mRNA Magnetic Isolation Module (New England BioLabs, Ipswich, MA, USA) combined with SMARTer Apollo NGS library prep system (Takara, Mountain View, CA, USA) for automated polyA RNA isolation. The NEBNext Ultra II Directional RNA Library Prep Kit (New England BioLabs) was used for library preparation under the PCR cycle number of 9. After library QC analysis and qPCR quantification, individually indexed and compatible libraries were proportionally pooled and sequenced using HiSeq platform (San Diego, CA, USA). Under the sequencing setting of single read 1×51 bp, about 25 million pass filter reads per sample were generated. Sequence reads were demultiplexed and exported to fastq files using CASAVA

1.8 software (Illumina). The sequencing data were submitted to the Sequence Read Archive (SRA) of National Center for Biotechnology Information (NCBI), and are accessible through the GEO accession number; GSE140926.

To analyze differential gene expression, sequence reads were aligned to the reference genome using the TopHat aligner, and reads aligning to each known transcript were counted using Bioconductor packages for next-generation sequencing data analysis. Sequence reads were demultiplexed and exported to fastq files using CASAVA 1.8 software (Illumina). Cuffdiff or DESeq2 was the tool used for differential expression. The differential expression analysis between different sample types was performed using the negative binomial statistical model of read counts as implemented in the edgeR Bioconductor software package. The cluster analysis of all genes differentially expressed in individual comparisons is performed using the Bayesian infinite mixture models, which was analyzed by The Laboratory for Statistical Genomics and Systems Biology at the University of Cincinnati.

2.6. Quantitative Real-Time RT-PCR (RT-qPCR)

Total RNA isolated (RNeasy Mini Kit, Qiagen Inc.) from normal skin pericytes, burn eschar pericytes, and dermal fibroblasts was subjected to RT-qPCR to analyze the expression levels of the target genes. Up to 400 ng of total RNA was used for cDNA synthesis using random primers (100 ng; Invitrogen) and a M-MLV reverse transcriptase (Invitrogen). All gene-specific probes were FAM Taqman MGB probes and used a Taqman Universal PCR Master Mix. Taqman probes for the following human gene products were purchased from Thermo Fisher: *FOXE1* (Hs00916085_s1), *POSTN* (HS01566750_m1), *ADAM12* (HS01106101_m1), *TGF-β1* (HS00998133_m1), *CD248* (endosialin; HS00535586_s1), *FN1* (HS01549976_m1), and *GAPDH* (Hs02786624-G1). *GAPDH* was used as a housekeeping gene control for all experiments. Real-time qPCR was performed using a StepOnePlus Real-Time PCR System using the following protocol: enzyme activation at 95 °C for 10 min, then 40 cycles of PCR at 95 °C for 15 s and 60 °C for 1 min. The comparative critical cycle (Ct) method was used to determine the expression levels of target genes after normalization to *GAPDH* expression. The data are presented as fold change pericyte expression levels compared to fibroblast expression ± SEM.

2.7. Cell Proliferation (MTT) Assay

Primary normal and burn eschar skin-derived pericytes (5×10^4) seeded on a 24 well plate were grown overnight in pericyte media (Zenbio). The following day, the cells were washed with 1× PBS and switched to DMEM media (Thermo Fisher) containing 0.1% dialyzed FBS for 24 h. Cells were then treated with or without TGF-β1 (PeproTech, Rocky Hill, NJ, USA) at a concentration of 10 ng/mL in 0.1% dialyzed FBS DMEM for another 24 h. After this treatment period, the MTT assay was performed using the CellTiter 96[®] Non-Radioactive Cell Proliferation Assay (Promega Corporation, Madison, WI, USA). Cells were placed in fresh media and dye solution according to the manufacturer and incubated at 37 °C for two hours, followed by the addition of solubilization/stop solution and another incubation for 1.5 h at 37 °C. Results were obtained using a SpectraMax 384 Plus plate reader (Molecular Devices, San Jose, CA, USA) at 570 nm of 200 μL aliquots placed into a Falcon Tissue Culture Treated 96 well plate. Optical densities were obtained using SoftMax Pro v3.1.2 software. Data are represented as fold change in proliferation ± SEM.

2.8. Enzyme-Linked Immunosorbent Assay (ELISA)

IL-6 and IL-8 human ELISA kits were purchased from Thermo Fisher Scientific and were run according to the manufacturer's instructions. Briefly, supernatant from pericytes grown in 6 well plates was collected in triplicate. Then, 50 μL of supernatant was added to each well along with 50 μL of biotinylated antibody reagent. The plate was covered and incubated at room temperature for two hours. Following washes, 100 μL of a streptavidin-HRP solution was added to each well and incubated at room temperature for 30 min. Following additional washes, 100 μL of TMB substrate solution was added to each well, incubated in the dark for 30 min, and the reaction was terminated with the addition

of 100 μ L stop solution. The plate was read at 450 nm using a SpectraMax 384 plate reader. Data are presented as an average concentration \pm SEM.

2.9. *In Vitro* Wound Healing Assay

Primary normal and burn eschar skin-derived pericytes were cultured to confluence in Falcon Tissue Culture Treated six-well plates and allowed to grow for 24 h at 37 °C. On each plate, a horizontal line was drawn across each well to image the same area consistently. The cells were then washed with 1 \times PBS and the media was changed to DMEM containing 0.1% dialyzed FBS and incubated for 24 h at 37 °C. Following this incubation, media was removed and using a P1000 pipet tip, a vertical wound was made across the monolayer of cells. Each well was then washed twice with 1 \times PBS and imaged for time zero. Cells were then changed to DMEM with 0.1% dialyzed FBS for 24 h at 37 °C. After this treatment period, the media was collected for future use, and the cells were washed twice with 1 \times PBS. A 24-h treatment image was taken. Using ImageJ software (NIH), the distance of the wounds was measured for both time zero and 24 h post-treatment. These distances were used to calculate % closure as such: (Time zero distance – 24-h distance/Time zero) distance \times 100. Cell migration was expressed as a fold change compared to no treatment cells \pm SEM.

2.10. Cell Contraction Assay

Primary normal and burn eschar pericytes along with fibroblasts were grown in cell culture flasks to a confluent monolayer, quiesced for 24 h in DMEM with 0.1% dialyzed FBS, trypsinized, and collected at a concentration of 2×10^6 cells/mL. The cells were mixed at a ratio of 2:8 with a collagen solution (Cell Bio Labs Inc. San Diego, CA, USA) and incubated for 1 h at 37 °C with 5% CO₂. After incubation, fresh DMEM with 0.1% dialyzed FBS was added on top of the collagen gels, and images were taken at time zero and again 24 h later. Cell contraction was measured using ImageJ-NIH software analysis, and data are presented as fold change contraction as compared to day 0 images \pm SEM.

2.11. Statistical Analysis

Statistical analysis of the RNA-seq data was performed by The Laboratory for Statistical Genomics and Systems Biology at the University of Cincinnati. RNA-seq results were considered significant with a false discovery rate (FDR) <0.1. All the other data are presented as mean \pm standard error of the mean. Student's t-test and One-way analysis of variance (ANOVA) were used and $p < 0.05$ was considered statistically significant.

3. Results

3.1. Isolation of Pericytes from Burn Eschar

Pericytes play an important role in the process of wound healing. Here we seek to isolate and characterize pericytes in the eschar of burn wounds. First, we characterized the morphology and phenotype of pericytes isolated from burn wounds. Pericytes were isolated from normal skin, or the burn wound eschar by flow cytometry using the following cell marker profiles; CD73+, CD105+ CD146+, CD34–, CD45–, and CD56–. After incubation in pericytes growth media the cells were analyzed by flow cytometry for the pericyte marker CD146 and NG2 and stem cell markers CD105 and CD73. The cells were also stained for the endothelial marker CD34 and skeletal muscle marker CD56. The majority of isolated cells express the pericytes markers CD146 (95%), CD73 (95%), CD105 (55%), and NG2 (23%) but not skeletal muscle (CD56) or endothelial (CD34) cells markers both less than 5% (Figure 1a) suggesting the isolated cells are pericytes. A study by van der Veen et al. isolated stem cells from burn eschar [39]. In this study, the stem cells isolated were positive for CD90, CD105 and CD73 and negative for CD31, CD45, CD14, and CD79a which have a similar CD expression profile to the cells that were isolated in the present study. Phase contrast images of pericytes isolated from both normal skin and burn eschar tissues display a cell body with a prominent nucleus containing

small amount of cytoplasm with several long processes (Figure 1b). To further verify that the isolated cells are pericytes, the cells were stained for pericyte markers CD146 and, NG2, as well as fibroblast marker S100A4 (Figure 2). Here we show that greater than 90% of the pericytes expressed CD146 and nearly all the pericytes stained for NG2 (Figure 2a–c). To verify whether fibroblast may have been isolated along with the pericytes the cells were analyzed for the expression of the fibroblast marker S100A4. High expression of S100A4 is seen on fibroblast (Figure 2a,d). Pericytes isolated from normal skin and burn eschar, showed only a few cells with a very low level of S100A4 staining (Figure 2d). When the pericytes isolated from the burn eschar were compared to normal skin pericytes, there was a slight increase in the number of S100A4 positive cells, but this increase was not significant (Figure 2d). Compared to fibroblasts the S100A4 staining in the pericytes was only $11.67\% \pm 3.85$; normal skin and $14.49\% \pm 4.51$; burn eschar (Figure 2d). Interestingly, pericytes isolated from burned eschar but not from normal skin showed expression of some smooth muscle markers such as SM22 but not MHY11 or Calponin-1 (Figure 2e). Compared to normal skin pericytes with no SM22 staining, pericytes isolated from burn eschar showed SM22 staining up to 60%. Meanwhile, another smooth muscle marker MHY11 or Calponin-1 was absent from pericytes isolated from either normal skin or burn eschar suggesting a plasticity of fate in burn eschar pericytes. Taken together the data indicates that the significant number of cells isolated are pericytes and these cells should have a MSC phenotype since they express the MSC markers CD90, CD105, and CD73.

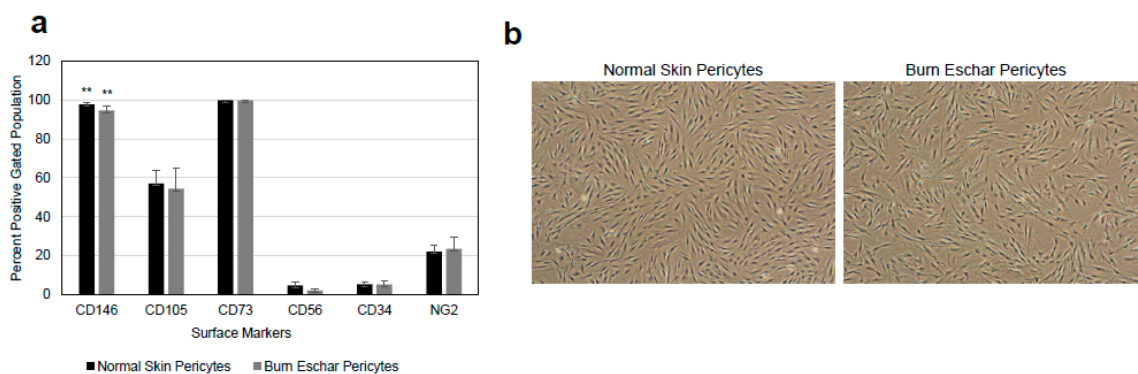


Figure 1. (a) Isolation and characterization of pericytes from skin. Cells grown in pericyte growth media were analyzed for the pericytes marker CD146 and neuron-gial 2 (NG2) and stem cell markers CD105 and CD73. The cells were also stained for the endothelial marker CD34 and skeletal muscle marker CD56. These cells did not express the endothelial marker CD34 or smooth muscle marker CD56 indicating that the isolated cell population are of pericyte lineage. Pericytes isolated from each of six different patients undergoing debridement after burn injury and breast reduction surgeries were used for flow analysis. Statistical analyses were performed using one-way analysis of variance (ANOVA) and $p < 0.05$ was considered statistically significant. $** p < 0.01$. (b) Shown are representative phase-contrast images of pericytes isolated from normal skin and burn eschar tissues.

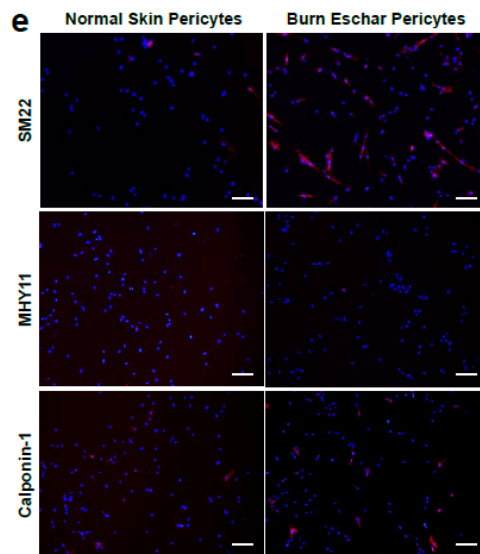
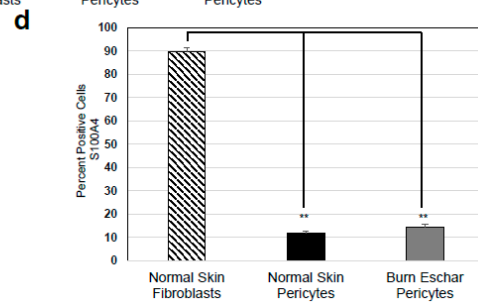
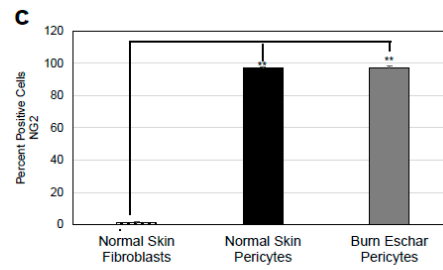
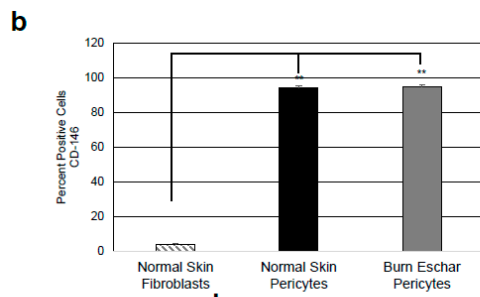
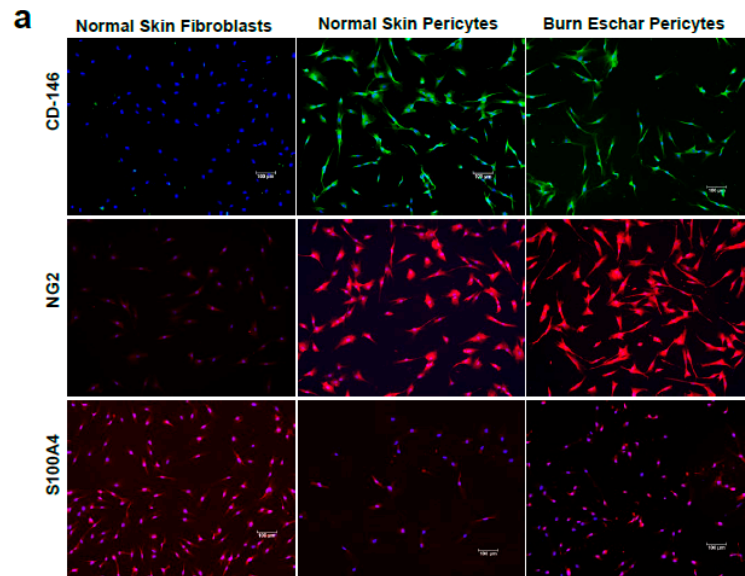


Figure 2. Isolated cells are a heterogeneous population of pericytes. (a) Cultured pericytes from normal skin and burn eschar were analyzed for expression of the pericyte markers CD146 and NG2 along with the fibroblast marker S100A4. Representative images of the experiments performed on three different cultures derived from three different patients for normal skin pericytes, burn eschar pericytes and fibroblasts are shown. Images were captured using Eclipse 90i microscope and photographed with a DS-Qi1MC Digital Microscope. Scale bar: 100 μ M. Quantitative analysis of (b) CD146, (c) NG2, and (d) S100A4 was performed. Quantitative analysis was performed in triplicate at 10x high powered fields using NIS-Elements AR3.1 software. Data represented as mean \pm SEM of two independent studies. Statistical analysis was performed using Student's *t* test with $p < 0.05$ considered statistically significant. ** $p < 0.01$. The results show pericytes are greater than 90% positive for CD146 and NG2 and less than 15% positive for S100A4. The fibroblasts are greater than 90% positive for S100A4 and less than 10% positive for CD146 and NG2. (e) Shown is the representative images on the staining performed on normal skin pericytes and burn eschar pericytes derived from two different patients using SM22, myosin smooth muscle heavy chain (MHY)11, and Calponin-1 are shown. Scale bar: 30 μ M.

3.2. Burn Eschar Pericytes Overexpress Inflammatory Cytokines

Next, we determine whether the burn environment affected pericytes gene expression. Using RNA-seq, we identified 443 differentially expressed genes between normal- and burn eschar-derived pericytes. While comparing normal skin pericytes to normal skin fibroblasts, we identified 1021 distinct genes, however comparing burn eschar pericytes to normal skin fibroblasts we identified 2449 differential genes (Supplemental Data S1). From these sets of genes, we identified six pro-inflammatory genes and two anti-inflammatory genes to be upregulated (Table 2) specifically in burn eschar pericytes. Using an ELISA assay, we analyzed the protein expression of these genes in normal skin and burn eschar derived pericytes. We found that both interleukin-6 (IL-6; 5 fold) and interleukin-8 (IL-8; 3.75 fold) protein levels were significantly higher in burn eschar pericytes than normal skin pericytes (Figure 3). Utilizing real-time RT-PCR analysis, we found that TGF- β 1 gene expression was significantly higher (38%) in the burn eschar derived pericytes than the normal skin-derived pericytes (Figure 4a). Rustenhoven et al. showed that TGF- β 1 treated pericytes induced the secretion of IL-6 [40]. In addition, they showed that pericyte stimulation with TGF- β 1 and IL-1 β has a synergistic release of IL-6 [40] which correlates with our finding that IL-1 β is upregulated (Table 2) and a 5 fold increase in IL-6 expression (Figure 3a). MyD88, an upstream regulator of interleukin-1 (IL-1) and tumor necrosis factor- α (TNF- α) expression [41,42] was also examined. We found expression of MyD88 was increased in the burn eschar derived-pericytes compared to normal skin derived-pericytes (Figure 4b). Although the increase did not reach significance, the results are suggestive that the burn eschar derived-pericytes increase pro-inflammatory cytokines in part through the activation of MyD88. A disintegrin and metalloprotease 12 (ADAM12) has been found to be upregulated in chronic ulcers and may contribute to a decrease in keratinocyte migration and proliferation [43,44]. Furthermore, ADAM12+ cells were found to be progenitors of collagen-overproducing cells [45]. When ADAM12 gene expression was examined, we found that expression was significantly greater (175%) in the burn eschar derived pericytes than the normal skin-derived pericytes (Figure 4c). These data suggest that the burn eschar stimulates pericyte secretion of the pro-inflammatory factors TGF- β 1 and IL-1 β . These factors further promote an enhanced secretion of pro-inflammatory cytokine IL-6. Taken together, burn eschar derived-pericytes have a pro-inflammatory phenotype. The overexpression of ADAM12 is suggestive of the possibility for pericyte differentiation into a pro-fibrotic phenotype.

Table 2. Expression profile of pro- and anti-inflammatory genes in burn eschar pericytes from RNA-seq analysis.

Pro-Inflammatory Genes	Fold Change	Ant-Inflammatory Genes	Fold Change
IL-6	6.74 ↑	NFκBIZ	2.50 ↑
IL-1β	48.39 ↑	NFκBIα	2.01 ↑
IL-1α	29.52 ↑		
IL-8 (CXCL8)	15.69 ↑		
TNFαIP3	8.38 ↑		
CXCL-14	0.16 ↓		

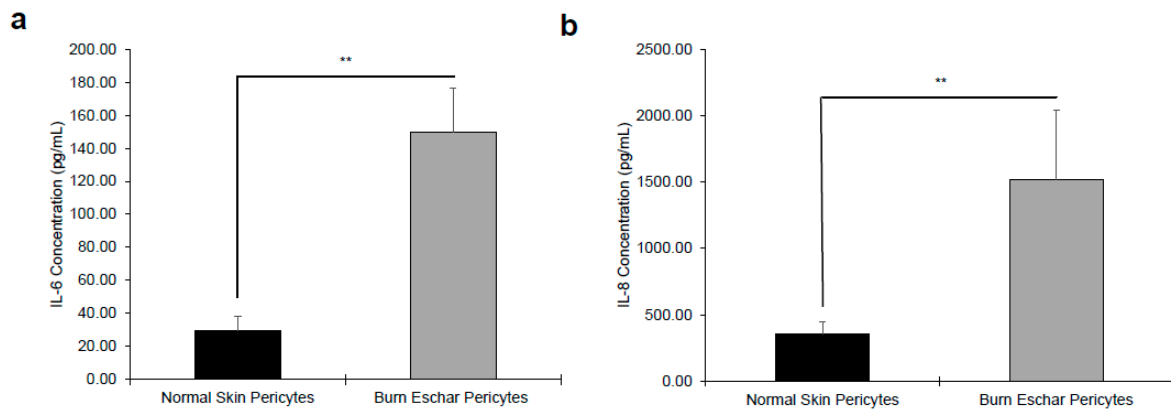


Figure 3. Burn Eschar pericytes express high levels of pro-inflammatory cytokines. ELISA analysis of (a) IL-6 and (b) IL-8 expression by normal and burn eschar pericytes. ELISA analysis was performed using normal skin pericytes derived from three different patients and burn eschar pericytes derived from four different patient samples. The results indicate that pericytes isolated from the burn eschar express significant higher amounts of the pro-inflammatory cytokines IL-6 and IL-8 compared to normal pericytes. Statistical analysis was performed using ANOVA with $p < 0.05$ considered statistically significant. Data is represented as mean \pm SEM values. ** $p < 0.01$. Interleukin- 1alpha (IL-1α); Tumor necrosis factor alpha-induced protein 3 (TNFαIP3); chemokine ligand- 14 (CXCL-14); nuclear factor of kappa light polypeptide gene enhancer in B cells inhibitor, zeta (NFκBIZ); nuclear factor of kappa light polypeptide gene enhancer in B cells inhibitor, alpha (NFκBIα).

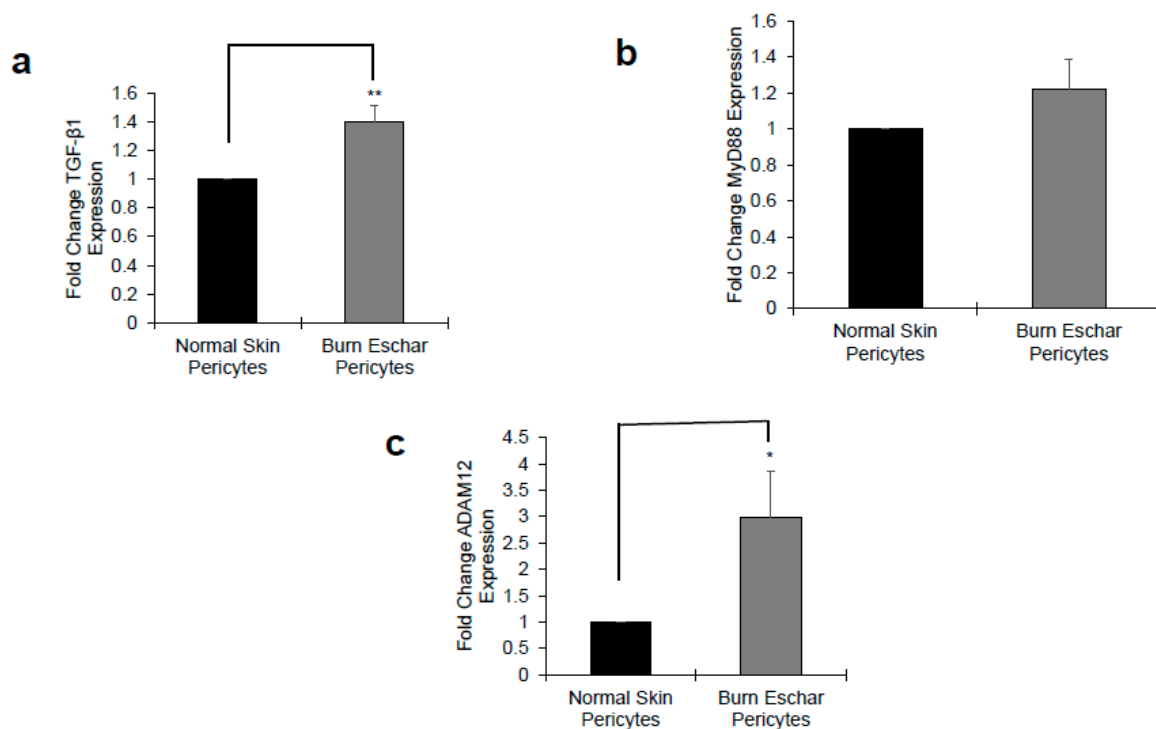


Figure 4. Burn eschar pericytes express high levels of pro-fibrotic genes. Normal and burn eschar pericytes were analyzed for transcription of (a) transforming growth factor (TGF)- β 1, (b) myeloid differentiation factor 88 (MyD88), and (c) A disintegrin and metalloprotease 12 (ADAM12) using real time RT-PCR. Burn eschar pericytes display significantly higher expression of TGF- β 1 and ADAM12 than normal pericytes. Statistical analysis was performed using ANOVA with $p < 0.05$ considered statistically significant. Values are means \pm SEM of three independent studies using three different cultures for both the cell types performed in triplicate. * $p < 0.05$; ** $p < 0.01$.

3.3. Burn Eschar Derived-Pericyte Express FOXE1

The expression of forkhead box E1 (FOXE1) has been primarily found in thyroid cells and is essential for thyroid development [46,47]. In our RNA-seq analysis, we found that FOXE1 expression was highly upregulated in both normal skin (601.95 fold increase) and burn eschar pericytes (1640.93 fold increase) when compared to fibroblasts (Supplemental Data S1). To verify the expression of FOXE1 in pericytes, real-time RT-PCR was performed. Here we show that FOXE1 expression in pericytes isolated from normal skin was minimal, but the expression in the pericytes from burn eschar was significantly higher (Figure 5a). There was a 12 fold increase in FOXE1 transcription in the burn eschar derived pericytes compared to normal skin pericytes (Figure 5a). Immunocytochemistry was performed on the cells to verify that this increase in mRNA expression translated to an increase in protein expression (Figure 5b). Quantification of cells expressing FOXE1 between normal skin pericytes and burn eschar pericytes showed that FOXE1 protein expression is significantly increased in burn eschar pericytes (Figure 5c). This is the first observation of FOXE1 expression in pericytes. The function of FOXE1 outside of the thyroid is not well understood. Since FOXE1 is involved in thyroid development and differentiation, it may play a role in regulating the differentiation state of pericytes during the wound healing process which will be investigated in future studies.

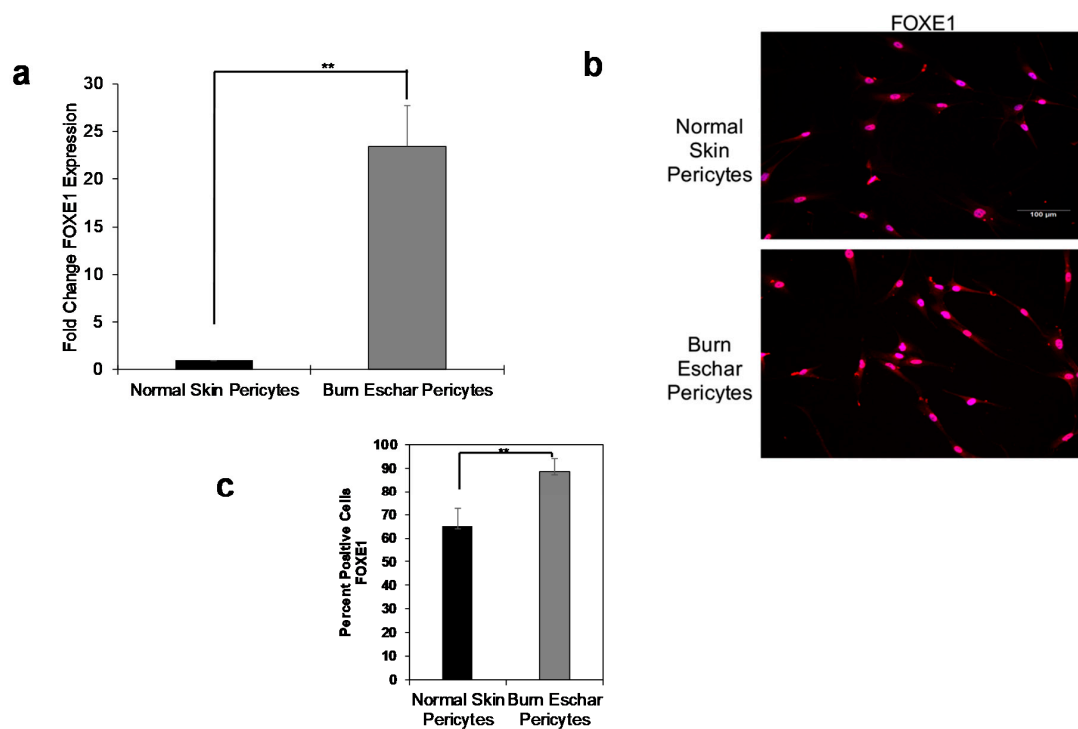


Figure 5. Pericytes express forkhead box E1 (FOXE1). (a) mRNA expression of FOXE1, (b) immunofluorescence of FOXE1 protein expression, and (c) Quantitative analysis of FOXE-1 protein expression. Both normal and burn eschar pericytes express FOXE1 but the burn eschar pericytes have a significantly greater expression of FOXE1 than normal pericytes. Three different cultures of pericytes derived from three different patients of normal skin and burn eschar tissues were utilized for real time RT-PCR; two different cultures of normal skin and burn eschar was used for immunofluorescence. Quantitative analysis was performed on FOXE1 stain in 3 10× high powered fields using NIS-Elements AR3.1 software. Data represented as mean ± SEM of two independent studies. Scale bar: 100 μM. Statistical analysis was performed using Student's *t* test with $p < 0.05$ considered statistically significant. ** $p < 0.01$.

3.4. Burn Eschar Derived-Pericyte Express Fibroblast Markers

Studies have shown that pericytes play a role in fibrosis by differentiating into a fibroblast-myofibroblast like phenotype. The signaling mechanisms that promote pericyte differentiation to a fibroblast-myofibroblast phenotype are not well understood. In RNAseq data, we found that fibronectin, endosialin, and periostin gene expression is overexpressed in burn eschar derived-pericytes (Supplemental Data S2). Using real-time RT-PCR, we found that the burn eschar derived-pericytes had a significant increase in fibronectin (FN1) expression (60%) compared to normal skin derived-pericytes (Figure 6a). Endosialin (CD248) is dynamically expressed on pericytes and fibroblasts during tissue development and inflammation. It has been shown that tissue with high endosialin mRNA expression has the protein present, whereas low mRNA expression fails to translate to protein detection [48]. A study by Smith et al. [49] found that endosialin knockout mice were protected from fibrosis due to less pericyte differentiation towards a myofibroblast phenotype. Here we show that pericytes isolated from burn eschar have a significantly (0.82 fold) higher expression of endosialin (CD248) mRNA than normal skin pericytes (Figure 6b). Periostin is a matricellular protein that has been found to play a role in dermal fibroblast proliferation and differentiation into myofibroblast [50–52]. Here we found that periostin gene expression was significantly higher (0.75 fold) in the burn eschar derived pericytes than normal skin pericytes (Figure 6c). When mRNA expression of periostin and fibronectin was compared between pericytes isolated from burn eschar and fibroblasts, we found the pericytes had a 15 fold increase in periostin (Figure 6d) and 3 fold increase in fibronectin

1 (Figure 6e). Next, periostin protein expression in vivo was determined. Healthy normal human skin or burn eschar were processed for histological analyses of pericytes and periostin. Tissues were incubated with CD146 and periostin antibody then visualized using fluorescent secondary antibodies. We show in normal skin, pericytes (green) had very little periostin (red) staining (Figure 6f). In the burn eschar, significant staining of periostin (red) was observed throughout the tissue (Figure 6f). The pericytes (green) in the burn eschar tissue had a high expression of periostin compared to normal skin pericytes (Figure 6f). Taken together these data are suggestive that the burn wound environment promotes the expression of genes and proteins in pericytes that are known mediators of fibroblast to myfibroblast transition.

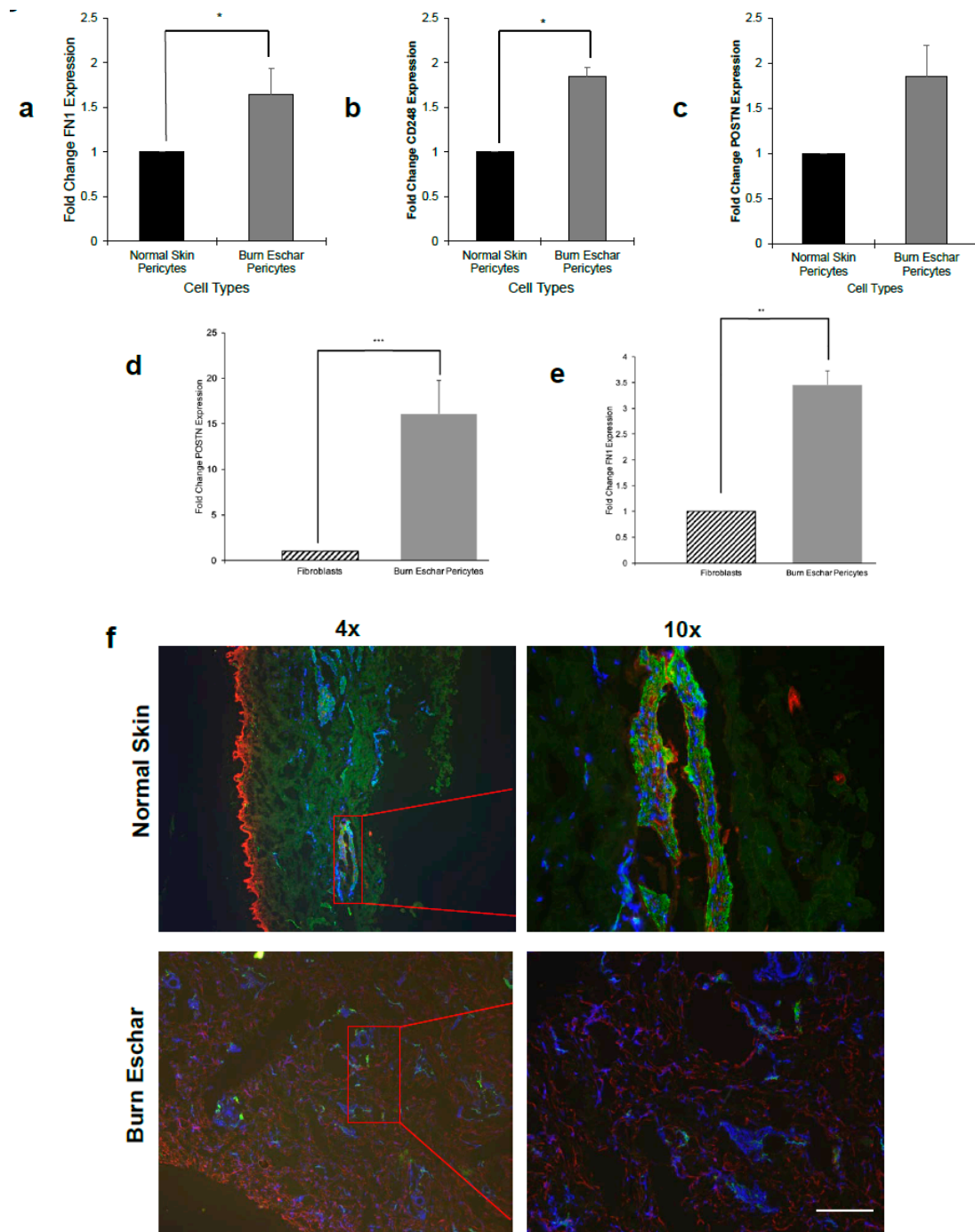


Figure 6. Burn eschar pericytes express fibrotic proteins. mRNA expression of (a) fibronectin (FN1), (b) endosialin (CD248), and (c) periostin (POSTN) between normal skin and burn eschar pericytes was determined using real time RT-PCR. mRNA expression of (d) periostin (POSTN) and (e) fibronectin (FN1) was compared between fibroblasts and pericytes using real time RT-PCR. (f) Immunohistochemistry of normal tissue and burn eschar was performed using antibodies directed towards pericytes (green), periostin (red), and nuclei (blue). Shown here are representative images of three different experiments performed on three different patient derived normal skin and burn eschar tissue sections. Scale bar: 100 μ M. These data show that expression of the fibrotic proteins fibronectin, endosialin and periostin is significantly higher in burn eschar pericytes compared to either normal pericytes or fibroblasts. Real time RT-PCR was performed using three cultures derived from normal skin, burn eschar, and normal fibroblasts were used. Data are presented as mean \pm SEM values of three independent experiments performed in triplicate. Statistical analysis was performed using ANOVA with $p < 0.05$ considered statistically significant. * $p < 0.05$; ** $p < 0.01$; *** $p < 0.001$.

3.5. Burn Eschar Derived-Pericytes Have an Increased Contractile Response

Here we determined whether the burn eschar isolated pericytes have a fibroblast-like phenotype by studying the functional properties of proliferation, migration, and contraction. Using the MTT assay we did not observe a difference in proliferation between fibroblast, pericytes isolated from normal skin or pericytes from burn eschar (Figure 7a). Using the scratch assay to analyze migration, we did not see a significant difference between fibroblasts and pericytes (Figure 7b). Since collagen contraction is one of the major functions of fibroblasts and myofibroblasts, we determined the ability of the cells to contract a collagen lattice. Here we show, pericytes isolated from the skin or burn eschar both had an increased ability to contract collagen compared to fibroblasts (Figure 8a). We show that the pericytes from normal skin had a 5 fold and pericytes from burn eschar had a 6 fold change in contraction compared to fibroblasts (Figure 8b). Taken together these data suggests that burn eschar pericytes possess the ability to contract the wound matrix.

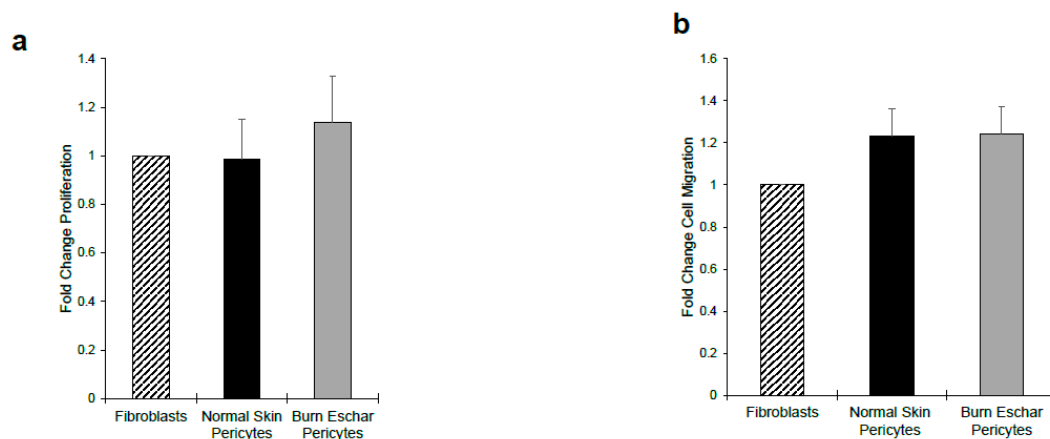


Figure 7. Cell proliferation and migration is unchanged between normal skin and burn eschar pericytes. Analysis of (a) cellular proliferation using the MTT assay and (b) in-vitro migration using the scratch assay shows no difference between normal and burn eschar pericytes. Cell proliferation assay was performed using five different cultures of normal skin- and burn eschar-derived pericytes and cell migration assay was performed using six different cultures each of normal skin- and burn eschar-derived pericytes. Statistical analysis was performed using one-way ANOVA with $p < 0.05$ considered statistically significant. Data is represented as mean \pm SEM values.

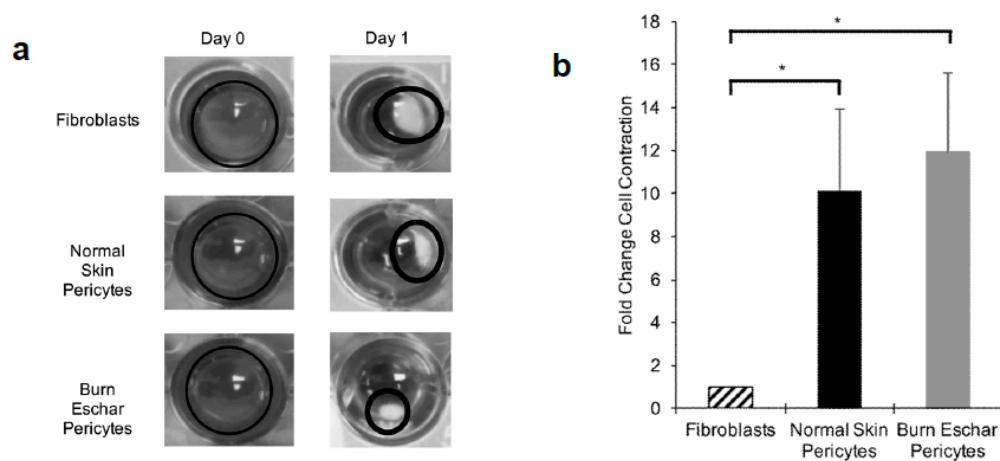


Figure 8. Burn eschar pericytes display increased cellular contractility. **(a)** Collagen contraction assay between fibroblasts and pericytes isolated from normal skin and burn eschar. Cellular contractile ability of normal skin pericytes and burn eschar pericytes was compared to normal skin-derived fibroblasts. Shown here is the representative images of three independent experiments performed in triplicate. **(b)** Quantitative analysis of contracted collagen lattice normalized to the average area of contraction seen in fibroblasts, set as a baseline value of 1. Each data point represents the mean \pm SEM of the averages of triplicate reads for each culture derived from the three different patient samples. Statistical significance was determined using one-way ANOVA. * $p < 0.05$. Data indicates that burn eschar pericytes have a greater contractile capability than fibroblast.

4. Discussion

The processes involved in wound healing that leads to normal tissue repair are well identified, but our understanding of how dysregulation of inflammatory and reparative cells leads to fibrosis is not well understood. The inflammatory process is required to promote wound healing, but an extended and persistent pro-inflammatory cascade leads to fibrotic scarring. Traditionally, the fibroblast and myofibroblast have been presumed to be the principal cell mediating fibrosis [53]. During the granulation phase of wound healing, local fibroblasts begin migrating from the periphery into the provisional scar tissue. As they move into the provisional matrix, they begin to differentiate into a cell phenotype known as myofibroblast, which are responsible for wound contraction. Upon closure of the wound, the myofibroblast undergoes apoptosis [54]. On the other hand, the persistence of myofibroblasts during the remodeling phase promotes hypertrophic scarring and leads to the development of fibrosis. Recent studies have indicated that other cells may be involved in fibrotic disease [55–57]. Pericytes are cells that have been found to possess stem cell-like properties with a capacity to differentiate into cell-states with pro-regenerative properties in addition to their essential role in regulating angiogenesis [20,25].

Pericytes are associated with the microvasculature and facilitate vascular stabilization, maintain vessel integrity and regulate vascular tone. During angiogenesis activated pericytes detach from the vessel to facilitate endothelial dissociation and initiation of angiogenesis then reattach to promote vessel stabilization and maturation. During wound healing pericytes have been found to detach from microvessels [11,58]. Pericyte detachment and subsequent activation is thought to promote dedifferentiation into a stem cell-like phenotype. In this state, pericytes have the potential to differentiate into various cells depending on cues from neighboring cells or interaction with specific signaling molecules [20,23,59]. The pluripotency of pericytes have made them a novel candidate for tissue repair. Pericytes implantation has been successful in repairing various tissues including muscle, heart, and brain [16,29,60,61]. Pericytes have also been implicated in promoting fibrosis in various tissues [36,37,55,62,63]. Studies by Birbrair et al. suggest two populations of pericytes type 1 and type 2 [64]. Type-1 pericytes when exposed to TGF- β are fibrogenic [35]. Type-2 pericytes were found to promote angiogenesis and tissue repair [60,65]. Understanding the signaling pathways that promotes

pericytes to a collagen producing phenotype, myofibroblast/fibroblast, will enable the modulation of pericytes into a more regenerative phenotype than a fibrotic-promoting state.

Fibrosis is an excessive amount of extracellular matrix (ECM) that accumulates in the wound tissue and leads to the loss of organ function. Fibrosis is viewed as excessive scar formation. During the granulation phase of wound healing, myofibroblasts initially deposit fibronectin and collagen III, forming the provisional matrix. Late in the granulation phase and the remodeling phase of wound healing, fibroblasts replace the provisional ECM with collagen I and elastin [66]. Fibrosis occurs when there is excessive production of ECM by myofibroblasts, which compromises normal tissue function, eventually leading to cell injury and death, which can further trigger myofibroblast activation continuing the fibrotic response cascade. Biologically active TGF β -1 is one of the major cytokines needed to generate α -SMA-positive myofibroblasts. Pathologies of over scarring or fibrosis include hypertrophic scars and keloids [67]. Recent studies have implicated pericytes in contributing to the fibrotic response [68,69]. Understanding the process and cells involved in fibrosis will allow for the identification of critical signaling pathways as potential therapeutic targets to circumvent fibrosis and promote normal tissue repair.

In the U.S., acute thermal injuries occur in over 2 million people a year. Of these, approximately 75,000 are hospitalized and about 14,000 die due to burn injury. World-wide an estimated 180,000 deaths a year are caused by burns [70]. Thermal burns over 20% of total body surface area results in burn shock which occurs in the first 18 hrs then there is a prolonged period of hypermetabolism and chronic inflammation which creates a high level of circulating cytokines [71]. Monocytes and neutrophils along with endothelial cells secrete the inflammatory cytokines TGF- β 1, TNF- α , IL-1, IL-6, IL-8, and MCP-1 after burn injury. Excessive production of these cytokines can lead to systemic inflammatory response syndrome. In the pericytes isolated from burn eschar, a significant increase in TGF- β 1, IL-1, and IL-6 was observed. This is highly suggestive that the wound environment is promoting pericytes secretion of inflammatory cytokines enhancing the inflammatory response. The mechanism promoting pericytes secretion of inflammatory cytokines will be useful in deducing the factors involved in excessive fibroplasia.

The main goals of this study were to characterize resident pericytes in burn eschar and determine whether these pericytes have distinct, identifiable characteristics. We have isolated pericytes from burn eschar (Figures 1 and 2) without enzymatic digestion and have shown differences exist between these cells and normal skin pericytes. The ability to isolate pericytes from wound eschar is of significant importance as it provides an avenue to characterize pericytes from different types of wounds and provides an opportunity to study the role and function of pericytes in different wound healing conditions. We show pericytes isolated from burn eschar have an increased expression of the pro-inflammatory cytokines IL-6 and IL-8 (Figure 3), TGF- β 1 (Figure 4), and IL-1 (Table 2). It is well established that TGF- β 1 is the main driver of contractile genes that promotes precursor cells to a myofibroblast phenotype [53]. TGF- β 1 induces p38 mediated activation of PI-3K-AKT pathway which confers apoptosis resistance [72]. It can activate the sonic Hedgehog pathway promoting transdifferentiation of hepatic stellate cells into myofibroblasts [73]. IL-1 β has been found to increase the expression of TGF- β 1 [74] and transform dermal microvascular endothelial cells into myofibroblasts [75]. Taken together, this suggesting that pericyte secretion of TGF- β 1 and IL-1 β could promote differentiation of precursor cell to a myofibroblast phenotype. MyD88, an upstream regulator of IL-1 and TNF- α has been shown to impair wound healing by upregulating the expression of pro-inflammatory cytokines and has been shown to contribute to fibrogenesis [76]. MyD88 is also upregulated in pericytes isolated from burn eschar (Figure 4). The activation of Toll-like receptor (TLR)/MyD88 signaling pathway is required for myofibroblast differentiation [76]. It is thought that MyD88 transduce profibrotic signaling through TGF- β receptor transactivation. Here we show that TGF- β 1 is upregulated in burn eschar pericytes (Figure 4). Thus, the expression of TGF- β 1 and IL-1 by pericytes can promote an autocrine enhancement of inflammatory pathways and potentially exacerbating fibrosis. It could be postulated that pericyte secretion of TGF- β 1 could promote an increased number of myofibroblasts found in the

wound. Further the possibility exists that high levels of TGF- β 1 may contribute to the differentiation of pericytes into myofibroblasts which has been observed in kidney fibrosis [77]. The role TGF- β 1 has on pericyte function in wound healing will be the focus of future studies.

We also show for the first time that pericytes from burn eschar express high levels of FOXE1, forkhead box E1 (Figure 5). This finding is of great interest since FOXE1, also known as thyroid transcription factor 2 (Ttf2), is a thyroid-specific transcription factor that belongs to the forkhead/winged-helix family that is essential for thyroid development [78]. The FOX proteins are a superfamily of conserved transcriptional regulators having a highly conserved forkhead box or winged helix DNA binding domain [79,80]. FOXE1 interacts with nucleosomes through its winged-helix DNA binding domain. In the thyroid, FOXE1 is essential during thyroid development and differentiation [81]. FOXE1 binds to promoters of 2 thyroid-specific genes (thyroglobulin and hydroperoxidase) and can act to promote and repress transcription of both genes [82–84]. A study by Fernández et al. identified 54 novel FOXE1 target genes, which include ADAMTS 9 and S100A4 [85]. A disintegrin and metalloproteinase with thrombospondin motifs (ADAMTS) 9 is involved in the binding of fibronectin and disrupting fibronectin fibrils [86]. S100A4 is involved in cell cycle progression and differentiation [87]. Here we show that S100A4 is highly expressed in fibroblast and virtually absent in normal skin pericytes (Figure 2). Although S100A4 expression in pericytes isolated from burn eschar is very low compared to fibroblasts, its expression is 25% higher compared to normal skin pericytes (Figure 2d). Thus, this increase in expression could contribute to modifying pericyte phenotype in burn wounds. These findings may suggest that the expression of FOXE1 in the burn eschar pericytes could be involved in S100A4 expression in pericytes isolated from burn eschar. Although we did not observe an upregulation of ADAMTS 9, we did observe a significant increase in ADAMT 12 mRNA expression (Figure 4c). It is not known if ADAMT 12 is a FOXE1 target gene, but overexpression of ADAMT 12 inhibits keratinocyte migration and proliferation causing impairment in wound healing [44]. Thus, overexpression of ADAMTS12 can contribute to the formation of chronic ulcers.

Phenotypically, pericytes from the burn eschar are found to express the fibroblast markers endosialin (CD248), periostin, and fibronectin 1 (Figure 6), which are known mediators of fibroblast to myofibroblast transition. Periostin is a matricellular protein found mainly in collagen-rich tissues, and expression is primarily associated with fibroblasts [50,88] and has been found to play a role in fibroblast proliferation and their differentiation into myofibroblast during wound repair [51,52]. During skin development, periostin is produced and is strongly related to pathological skin remodeling [89]. Yamaguchi et al. showed that serum levels of periostin correlated with fibroblast infiltration in patients with systemic sclerosis [90]. Recently, macrophage/monocyte infiltration has shown to be facilitated by periostin [69], and it can regulate keratinocyte differentiation and proliferation [91]. Periostin is a ligand for integrin α β 3, which promotes activation of FAK/PI3K/Akt pathway [92]. In renal disease, periostin mediates the phosphorylation of FAK, p38, and Erk [93]. During cutaneous wound healing, periostin protein expression is observed at day 3 and peaks between days 7 to 10 [51,52]. Thus, periostin may play a role in ECM remodeling and regulation of inflammation during wound healing. Here we show that periostin mRNA expression in pericytes from burn eschar is two-fold higher than normal skin pericytes (Figure 6c) and fifteen-fold higher than fibroblasts (Figure 6d). These data may suggest that upregulation of periostin in pericytes could modulate pericytes to a myofibroblast phenotype.

To our knowledge, this is the first study to isolate and characterize pericytes from burn wounds. Our findings from this study suggest that the wound environment plays a critical role in regulating the function and phenotype of pericytes during the healing process. Our data suggest that pericytes isolated from burn eschar differentiate into a fibroblast/myofibroblast phenotype due to the high expression of MyD88, fibronectin, periostin, and endosialin. Thus, these pericytes may contribute to fibrosis. In previous studies, including ours, have demonstrated that pericytes play a role in enhancing the wound healing process [28,94–96]. The difference between these previous studies and this study is the wound environment. These previous studies looked at pericyte function in excision wounds, which do not incur a significant inflammatory response nor significant tissue damage. This study examined

pericytes from acute burn wounds incurring severe tissue damage with increased inflammatory response. Understanding the factors and signaling pathways contributing to the differentiation of pericytes into a fibroblast-like cell may provide a novel treatment to significantly reduce or eliminate fibrosis in burn scars.

This study is also the first to identify the expression of FOXE1 in pericytes isolated from normal skin and burn eschar. This is of great interest since FOXE1 is a regulator of gene expression and essential for thyroid development and differentiation. FOXE1 is predominantly expressed in the thyroid but expression has also been found in colon, lung, and orofacial tissue [97–99]. FOXE1 has not been observed to play a role in fibrosis but a number of FOX members have shown to be involved in fibrosis. FOXO1 has been shown to enhance the Wnt/ β -catenin signaling pathway promoting the expression of collagen, α -SMA and fibronectin [100]. In heart, cardiac fibroblasts differentiate into myofibroblasts in a FOXO1 dependent manner [101]. Further, authors show that TGF- β induced the activation of FOXO1. In skin, knockdown of FOXO1 enhanced wound healing through enhanced keratinocyte migration, reduced inflammatory response and decreased collagen density [102]. FOXE1 may play a key role in pericyte differentiation into various phenotypes or the secretion of collagen. Very little is known regarding the signaling pathways involved in the differentiation of pericytes into other cell lineages. Thus, activation of FOXE1 may be a contributing factor to pericyte-myofibroblast differentiation. Understanding the expression and function of FOXE1 in pericytes will further our understanding of the signaling pathways regulating pericyte function. Further studies will be performed to analyze FOXE1 function and its implication on pericyte differentiation.

5. Conclusions

We report here for the first time that pericytes can be isolated from discarded normal skin and burn eschar tissues without the utility of the enzyme digestion process. We show that pure population of pericytes can be obtained, which can be utilized for biological analyses. Our studies show significant differences in the gene expression between normal skin pericytes and burn pericytes. We also observed a significant difference in gene expression patterns between fibroblasts and pericytes leading to the identification of the gene FOXE-1. FOXE-1 expression was noted specifically in pericytes, which may serve as a new marker for identifying skin pericytes. We also provide evidence that pericytes isolated from burn eschar express high levels of the inflammatory cytokines namely, TGF- β 1, IL-6, and IL-8. It is well established that these cytokines/chemokines play a significant role in fibrosis. In addition, previous studies, have demonstrated that pericytes have the ability to express collagen and differentiate into a myofibroblast phenotype. Our results show that pericytes from burn wounds, express higher levels of pro-inflammatory cytokines, and may be a source of myofibroblasts contributing to burn scar contractures.

Supplementary Materials: The following are available online at <http://www.mdpi.com/2077-0383/9/2/606/s1>, Supplemental Data S1 (a): List of significant genes identified using RNA-seq analysis comparing normal skin fibroblasts to normal skin pericytes, Supplemental Data S1 (b): List of significant genes identified using RNA-seq analysis comparing normal skin fibroblasts to burn eschar pericytes, Supplemental Data S2: List of significant genes identified using RNA-seq analysis comparing normal skin pericytes and burn eschar pericytes.

Author Contributions: L.S. conceived the ideas and designed the study; A.E., L.S., and R.J.B. planned the experiments; A.E. performed all the in-vitro studies; S.G. performed histology; X.Z. performed the RNA-seq experiments and comments; A.B. and M.J.I. performed immunocytochemistry. The University of Cincinnati Genomics Core Facility analyzed the RNA-seq data. RNA-seq data and provided statistically significant genes and comments. L.S., O.K., and R.J.B. participated in the scientific discussion and provided feedback. A.E., R.J.B., and L.S. interpreted the results. L.S. and R.J.B. wrote the manuscript; O.K. and X.Z. provided critical comments on the manuscript. All authors have read and agreed to the published version of the manuscript.

Funding: The work was supported in part by the start-up funds (#81220-CIN-17) from Shriners Hospitals for Children to L.S. Additional support was provided through a grant funding (#85118-CIN-18) from Shriners Hospitals for Children awarded to L.S. for these studies. L.S. and O.K. thank the support provided through an internal grant for these studies from the University of Cincinnati.

Acknowledgments: The authors gratefully acknowledge the technical assistance of Karen Dominico in the Shriners Hospitals for Children-Cincinnati Flow Cytometry Special Shared Facility and Mary Rolfes in the Shriners

Hospitals for Children-Cincinnati Histology Special Shared Facility. In addition, we thank Dorothy Supp, Petra Warner, Laura Fowler, and Judith Nelson for their assistance in procurement of the discarded tissue samples.

Conflicts of Interest: The authors declare no competing financial interest.

References

1. Karppinen, S.M.; Heljasvaara, R.; Gullberg, D.; Tasanen, K.; Pihlajaniemi, T. Toward understanding scarless skin wound healing and pathological scarring. *F1000Research* **2019**, *8*, 787. [[CrossRef](#)]
2. Ripa, A.L.; Kalabusheva, E.P.; Vorotelyak, E.A. Regeneration of Dermis: Scarring and Cells Involved. *Cells* **2019**, *8*, 607. [[CrossRef](#)] [[PubMed](#)]
3. Knittel, T.; Dinter, C.; Kobold, D.; Neubauer, K.; Mehde, M.; Eichhorst, S.; Ramadori, G. Expression and regulation of cell adhesion molecules by hepatic stellate cells (HSC) of rat liver: Involvement of HSC in recruitment of inflammatory cells during hepatic tissue repair. *Am. J. Pathol.* **1999**, *154*, 153–167. [[CrossRef](#)]
4. Shammout, B.; Johnson, J.R. Pericytes in Chronic Lung Disease. *Adv. Exp. Med. Biol.* **2019**, *1147*, 299–317. [[PubMed](#)]
5. Shaw, I.; Rider, S.; Mullins, J.; Hughes, J.; Péault, B. Pericytes in the renal vasculature: Roles in health and disease. *Nat. Rev. Nephrol.* **2018**, *14*, 521–534. [[CrossRef](#)] [[PubMed](#)]
6. Greenhalgh, S.N.; Conroy, K.P.; Henderson, N.C. Healing scars: Targeting pericytes to treat fibrosis. *QJM Int. J. Med.* **2015**, *108*, 3–7. [[CrossRef](#)] [[PubMed](#)]
7. Strudwick, X.C.; Cowin, A.J. The Role of the Inflammatory Response in Burn Injury. In *Hot Topics in Burn Injuries*; Karal, S.P., Ed.; IntechOpen: London, UK, 2017; pp. 37–57.
8. Bergers, G.; Song, S. The role of pericytes in blood-vessel formation and maintenance. *Neuro-Oncology* **2005**, *7*, 452–464. [[CrossRef](#)]
9. Stefanska, A.; Péault, B.; Mullins, J.J. Renal pericytes: Multifunctional cells of the kidneys. *Pflugers Arch. Eur. J. Physiol.* **2013**, *465*, 767–773. [[CrossRef](#)]
10. Goumans, M.J.; Valdimarsdottir, S.; Itoh, A.; Rosendahl, P.; Sideras, P.; ten Dijke, P. Balancing the activation state of the endothelium via two distinct TGF-beta type I receptors. *EMBO J.* **2002**, *21*, 1743–1753. [[CrossRef](#)]
11. Bodnar, R.J.; Wells, A. Pericyte regulation of vascular remodeling through the CXC receptor 3. *Arterioscler. Thromb. Vasc. Biol.* **2013**, *33*, 2818–2829. [[CrossRef](#)]
12. Bodnar, R.J.; Wells, A. Differential regulation of pericyte function by the CXC receptor 3. *Wound Repair Regen.* **2015**, *23*, 785–796. [[CrossRef](#)] [[PubMed](#)]
13. Yan, M.; Hu, M.; Yao, M.; Bao, S.; Fang, Y. GM-CSF ameliorates microvascular barrier integrity via pericyte-derived Ang-1 in wound healing. *Wound Repair Regen.* **2017**, *25*, 933–943. [[CrossRef](#)] [[PubMed](#)]
14. Gaceb, A.; Ozen, T.; Padel, M.; Barbariga, M.; Paul, G. Pericytes secrete pro-regenerative molecules in response to platelet-derived growth factor-BB. *J. Cereb. Blood Flow Metab.* **2018**, *38*, 45–57. [[CrossRef](#)] [[PubMed](#)]
15. Jansson, D.; Rustenhoven, J.; Feng, S.; Hurley, D.; Oldfield, R.L.; Bergin, P.S.; Mee, E.W.; Faull, R.L.; Dragunow, M. A role for human brain pericytes in neuroinflammation. *J. Neuroinflamm.* **2014**, *11*, 104. [[CrossRef](#)]
16. Crisan, M.; Corselli, M.; Chen, W.C.; Péault, B. Perivascular cells for regenerative medicine. *J. Cell Mol. Med.* **2012**, *16*, 2851–2860. [[CrossRef](#)]
17. Berger, M.; Bergers, G.; Arnold, B.; Hammerling, G.J.; Ganss, R. Regulator of G-protein signaling-5 induction in pericytes coincides with active vessel remodeling during neovascularization. *Blood* **2005**, *105*, 1094–1101. [[CrossRef](#)]
18. Chen, C.W.; Corselli, M.; Péault, B.; Huard, J. Human blood-vessel-derived stem cells for tissue repair and regeneration. *J. Biomed. Biotechnol.* **2012**, *2012*, 597439. [[CrossRef](#)]
19. de Souza, L.E.; Malta, T.M.; Kashima Haddad, S.; Covas, D.T. Mesenchymal Stem Cells and Pericytes: To What Extent Are They Related? *Stem Cells Dev.* **2016**, *25*, 1843–1852. [[CrossRef](#)]
20. Dulmovits, B.M.; Herman, I.M. Microvascular remodeling and wound healing: A role for pericytes. *Int. J. Biochem. Cell Biol.* **2012**, *44*, 1800–1812. [[CrossRef](#)]
21. Caplan, A.I. All MSCs are pericytes? *Cell Stem Cell* **2008**, *3*, 229–230. [[CrossRef](#)]
22. Bodnar, R.J.; Satish, L.; Yates, C.C.; Wells, A. Pericytes: A newly recognized player in wound healing. *Wound Repair Regen.* **2016**, *24*, 204–214. [[CrossRef](#)] [[PubMed](#)]
23. Mills, S.J.; Cowin, A.J.; Kaur, P. Pericytes, mesenchymal stem cells and the wound healing process. *Cells* **2013**, *2*, 621–634. [[CrossRef](#)] [[PubMed](#)]

24. Bodnar, R.J.; Satish, L. Targeting Pericytes to Improve Wound Healing Outcomes. *Curr. Pathobiol. Rep.* **2018**, *6*, 117–123. [[CrossRef](#)]
25. Thomas, H.; Cowin, A.J.; Mills, S.J. The Importance of Pericytes in Healing: Wounds and other Pathologies. *Int. J. Mol. Sci.* **2017**, *18*, 1129. [[CrossRef](#)]
26. Gaengel, K.; Genove, A.; Armulik, A.; Betsholtz, C. Endothelial-mural cell signaling in vascular development and angiogenesis. *Arterioscler. Thromb. Vasc. Biol.* **2009**, *29*, 630–638. [[CrossRef](#)]
27. Kutcher, M.E.; Herman, I.M. The pericyte: Cellular regulator of microvascular blood flow. *Microvasc. Res.* **2009**, *77*, 235–246. [[CrossRef](#)]
28. Bodnar, R.J.; Yang, T.; Rigatti, L.H.; Liu, F.; Evdokiou, A.; Kathju, S.; Satish, L. Pericytes reduce inflammation and collagen deposition in acute wounds. *Cytotherapy* **2018**, *20*, 1046–1060. [[CrossRef](#)]
29. Chen, C.W.; Okada, M.; Proto, J.D.; Gao, X.; Sekiya, N.; Beckman, S.A.; Corselli, M.; Crisan, A.; Saparov, A.; Tobita, K.; et al. Human pericytes for ischemic heart repair. *Stem Cells* **2013**, *31*, 305–316. [[CrossRef](#)]
30. Proebstl, D.; Voisin, M.B.; Woodfin, A.; Whiteford, J.; D'Acquisto, F.; Jones, G.E.; Rowe, D.; Nourshargh, S. Pericytes support neutrophil subendothelial cell crawling and breaching of venular walls in vivo. *J. Exp. Med.* **2012**, *209*, 1219–1234. [[CrossRef](#)]
31. Tu, Z.; Li, Y.; Smith, D.S.; Sheibani, N.; Huang, S.; Kern, T.; Lin, F. Retinal pericytes inhibit activated T cell proliferation. *Investig. Ophthalmol. Vis. Sci.* **2011**, *52*, 9005–9010. [[CrossRef](#)]
32. Paquet-Fifield, S.; Schluter, H.; Li, A.; Aitken, T.; Gangatirkar, P.; Blashki, D.; Koelmeyer, N.; Pouliot, N.; Palatsides, M.; Ellis, S. A role for pericytes as microenvironmental regulators of human skin tissue regeneration. *J. Clin. Invest.* **2009**, *119*, 2795–2806. [[CrossRef](#)] [[PubMed](#)]
33. Sundberg, C.; Ljungstrom, M.; Lindmark, G.; Gerdin, B.; Rubin, K. Microvascular pericytes express platelet-derived growth factor-beta receptors in human healing wounds and colorectal adenocarcinoma. *Am. J. Pathol.* **1993**, *143*, 1377–1388. [[PubMed](#)]
34. Stark, K.; Eckart, A.; Haidari, S.; Tirniceriu, A.; Lorenz, M.; von Bruhl, M.L.; Gartner, F.; Khandoga, A.G.; Legate, K.R.; Pless, R.; et al. Capillary and arteriolar pericytes attract innate leukocytes exiting through venules and 'instruct' them with pattern-recognition and motility programs. *Nat. Immunol.* **2013**, *14*, 41–51. [[CrossRef](#)] [[PubMed](#)]
35. Birbrair, A.; Zhang, T.; Files, D.C.; Mannava, S.; Smith, T.; Wang, Z.M.; Messi, M.L.; Mintz, A.; Delbono, O. Type-1 pericytes accumulate after tissue injury and produce collagen in an organ-dependent manner. *Stem Cell Res. Ther.* **2014**, *5*, 122. [[CrossRef](#)]
36. Lin, S.L.; Kisseleva, T.; Brenner, D.A.; Duffield, J.S. Pericytes and perivascular fibroblasts are the primary source of collagen-producing cells in obstructive fibrosis of the kidney. *Am. J. Pathol.* **2008**, *173*, 1617–1627. [[CrossRef](#)]
37. Mederacke, I.; Hsu, C.C.; Troger, J.S.; Huebener, P.; Mu, X.; Dapito, D.H.; Pradere, J.P.; Schwabe, R.F. Fate tracing reveals hepatic stellate cells as dominant contributors to liver fibrosis independent of its aetiology. *Nat. Commun.* **2013**, *4*, 2823. [[CrossRef](#)]
38. Boyce, S.T. Methods for the Serum-Free Culture of Keratinocytes and Transplantation of Collagen-GAG-Based Skin Substitutes. *Methods Mol. Med.* **1999**, *18*, 365–389.
39. Van der Veen, V.C.; Vlig, M.; van Milligen, F.J.; de Vries, S.I.; Middelkopp, E.; Ulrich, M.M. Stem cells in burn eschar. *Cell Transpl.* **2012**, *21*, 933–942. [[CrossRef](#)]
40. Rustenhoven, J.; Aalderink, M.; Scotter, E.L.; Oldfield, R.L.; Bergin, P.S.; Mee, E.W.; Graham, E.S.; Faull, R.L.; Curtis, M.A.; Park, T.I.; et al. TGF-beta1 regulates human brain pericyte inflammatory processes involved in neurovasculature function. *J. Neuroinflammation.* **2016**, *13*, 37. [[CrossRef](#)]
41. Du, X.; Shi, R.; Wang, Y.; We, W.; Sun, S.; Dai, Z.; Chen, C.; Weng, Z.; Li, X.; Liu, Q.; et al. Isoforskolin and forskolin attenuate lipopolysaccharide-induced inflammation through TLR4/MyD88/NF-kappaB cascades in human mononuclear leukocytes. *Phytother. Res.* **2019**, *33*, 602–609. [[CrossRef](#)]
42. Michaudel, C.; Mailliet, I.; Fauconnier, L.; Quesniaux, V.; Chung, K.F.; Wiegman, C.; Peter, D.; Ryffel, B. Interleukin-1alpha Mediates Ozone-Induced Myeloid Differentiation Factor-88-Dependent Epithelial Tissue Injury and Inflammation. *Front. Immunol.* **2018**, *9*, 916. [[CrossRef](#)] [[PubMed](#)]
43. Harsha, A.; Stojadinovic, H.; Brem, A.; Sehara-Fujisawa, A.; Wewer, U.; Loomis, C.A.; Blobel, C.P.; Tomic-Canic, M. ADAM12: A potential target for the treatment of chronic wounds. *J. Mol. Med.* **2008**, *86*, 961–969. [[CrossRef](#)] [[PubMed](#)]
44. Kawaguchi, M.; Hearing, V.J. The Roles of ADAMs Family Proteinases in Skin Diseases. *Enzyme Res.* **2011**, *2011*, 482498. [[CrossRef](#)] [[PubMed](#)]

45. Dulauroy, S.; Di Carlo, S.E.; Langa, F.; Langa, F.; Eberl, G.; Peduto, L. Lineage tracing and genetic ablation of ADAM12(+) perivascular cells identify a major source of profibrotic cells during acute tissue injury. *Nat. Med.* **2012**, *18*, 1262–1270. [[CrossRef](#)] [[PubMed](#)]
46. Carlsson, P.; Mahlapuu, M. Forkhead transcription factors: Key players in development and metabolism. *Dev. Biol.* **2002**, *250*, 1–23. [[CrossRef](#)]
47. Fernandez, L.P.; Lopez-Marquez, A.; Santisteban, P. Thyroid transcription factors in development, differentiation and disease. *Nat. Rev. Endocrinol.* **2015**, *11*, 29–42. [[CrossRef](#)]
48. Dolznig, H.; Schweifer, N.; Puri, C.; Kraut, N.; Rettig, W.J.; Kerjaschki, D.; Garin-Chesa, P. Characterization of cancer stroma markers: In silico analysis of an mRNA expression database for fibroblast activation protein and endosialin. *Cancer Immun.* **2005**, *5*, 10.
49. Smith, S.W.; Croft, A.P.; Morris, H.L.; Naylor, A.J.; Huso, D.L.; Isacke, C.M.; Savage, C.O.; Buckley, C.D. Genetic Deletion of the Stromal Cell Marker CD248 (Endosialin) Protects against the Development of Renal Fibrosis. *Nephron* **2015**, *131*, 265–277. [[CrossRef](#)]
50. Crawford, J.; Nygard, K.; Gan, B.S.; O’Gorman, D.B. Periostin induces fibroblast proliferation and myofibroblast persistence in hypertrophic scarring. *Exp. Dermatol.* **2015**, *24*, 120–126. [[CrossRef](#)]
51. Elliott, C.G.; Wang, J.; Guo, X.; Xu, S.W.; Eastwood, M.; Guan, J.; Leask, A.; Conway, S.J.; Hamilton, D.W. Periostin modulates myofibroblast differentiation during full-thickness cutaneous wound repair. *J. Cell Sci.* **2012**, *125 Pt 1*, 121–132. [[CrossRef](#)]
52. Ontsuka, K.; Kotobuki, Y.; Shiraiishi, H.; Serada, S.; Ohta, S.; Tanemura, A.; Yang, L.; Fujimoto, M.; Arima, K.; Suzuki, S.; et al. Periostin, a matricellular protein, accelerates cutaneous wound repair by activating dermal fibroblasts. *Exp. Dermatol.* **2012**, *21*, 331–336. [[CrossRef](#)] [[PubMed](#)]
53. Bochaton-Piallat, M.L.; Gabbiani, G.; Hinz, B. The myofibroblast in wound healing and fibrosis: Answered and unanswered questions. *F1000Research* **2016**, *5*, 752. [[CrossRef](#)] [[PubMed](#)]
54. Desmouliere, A.; Redard, M.; Darby, I.; Gabbiani, G. Apoptosis mediates the decrease in cellularity during the transition between granulation tissue and scar. *Am. J. Pathol.* **1995**, *146*, 56–66. [[PubMed](#)]
55. Di Benedetto, P.; Ruscitti, P.; Liakouli, P.; Cipriani, P.; Giacomelli, R. The Vessels Contribute to Fibrosis in Systemic Sclerosis. *Isr. Med. Assoc. J.* **2019**, *21*, 471–474.
56. Frangogiannis, N.G. Cardiac fibrosis: Cell biological mechanisms, molecular pathways and therapeutic opportunities. *Mol. Asp. Med.* **2019**, *65*, 70–99. [[CrossRef](#)]
57. To, S.; Agarwal, S.K. Macrophages and cadherins in fibrosis and systemic sclerosis. *Curr. Opin. Rheumatol.* **2019**, *31*, 582–588. [[CrossRef](#)] [[PubMed](#)]
58. Lin, S.L.; Chang, F.C.; Schrimpt, C.; Chen, Y.T.; Wu, C.F.; Wu, V.C.; Chiang, W.C.; Kuhnert, F.; Kuo, C.J.; Chen, Y.M.; et al. Targeting endothelium-pericyte cross talk by inhibiting VEGF receptor signaling attenuates kidney microvascular rarefaction and fibrosis. *Am. J. Pathol.* **2011**, *178*, 911–923. [[CrossRef](#)]
59. Chen, Y.T.; Chang, F.C.; We, C.F.; Chou, Y.H.; Hsu, H.L.; Chiang, W.C.; Shen, J.; Chen, Y.M.; Wu, K.D.; Tsai, T.J.; et al. Platelet-derived growth factor receptor signaling activates pericyte-myofibroblast transition in obstructive and post-ischemic kidney fibrosis. *Kidney Int.* **2011**, *80*, 1170–1181. [[CrossRef](#)]
60. Birbrair, A.; Zhang, T.; Wang, Z.M.; Messi, M.L.; Mintz, A.; Delbono, O. Pericytes at the intersection between tissue regeneration and pathology. *Clin. Sci.* **2015**, *128*, 81–93. [[CrossRef](#)]
61. Ishitsuka, K.; Ago, T.; Arimura, K.; Nakamura, K.; Tokami, H.; Makihara, N.; Kuroda, J.; Kamouchi, M.; Kitazono, T. Neurotrophin production in brain pericytes during hypoxia: A role of pericytes for neuroprotection. *Microvasc. Res.* **2012**, *83*, 352–359. [[CrossRef](#)]
62. Castellano, G.; Stasi, A.; Franzin, R.; Sallustio, F.; Divella, C.; Spinelli, A.; Netti, G.S.; Fiaccadori, E.; Cantaluppi, V.; Crovace, A.; et al. LPS-Binding Protein Modulates Acute Renal Fibrosis by Inducing Pericyte-to-Myofibroblast Trans-Differentiation through TLR-4 Signaling. *Int. J. Mol. Sci.* **2019**, *20*, 3682. [[CrossRef](#)] [[PubMed](#)]
63. Sava, P.; Ramanathan, A.; Dobronyi, A.; Peng, X.; Sun, H.; Ledesma-Mendoza, A.; Herzog, E.L.; Gonzalez, A.L. Human pericytes adopt myofibroblast properties in the microenvironment of the IPF lung. *JCI Insight* **2017**, *2*, e96352. [[CrossRef](#)] [[PubMed](#)]
64. Birbrair, A.; Zhang, T.; Wang, Z.M.; Messi, M.L.; Olson, J.D.; Mintz, A.; Delbono, O. Skeletal muscle pericyte subtypes differ in their differentiation potential. *Stem Cell Res.* **2013**, *10*, 67–84. [[CrossRef](#)]
65. Birbrair, A.; Zhang, T.; Wang, Z.M.; Messi, M.L.; Olson, J.D.; Mintz, A.; Delbon, O. Type-2 pericytes participate in normal and tumoral angiogenesis. *Am. J. Physiol. Cell Physiol.* **2014**, *307*, C25–C38. [[CrossRef](#)] [[PubMed](#)]

66. Xue, M.; Jackson, C.J. Extracellular Matrix Reorganization During Wound Healing and Its Impact on Abnormal Scarring. *Adv. Wound Care* **2015**, *4*, 119–136. [[CrossRef](#)] [[PubMed](#)]
67. Robles, D.T.; Berg, D. Abnormal wound healing: Keloids. *Clin. Dermatol.* **2007**, *25*, 26–32. [[CrossRef](#)] [[PubMed](#)]
68. Goritz, C.; Dias, D.O.; Tomilin, N.; Barbacid, M.; Shupliakov, O.; Frisen, J. A pericyte origin of spinal cord scar tissue. *Science* **2011**, *333*, 238–242. [[CrossRef](#)]
69. Yokota, K.; Kobayakawa, K.; Saito, T.; Hara, M.; Kijima, K.; Ohkawa, Y.; Harada, A.; Okazaki, K.; Ishihara, K.; Yoshida, S.; et al. Periostin Promotes Scar Formation through the Interaction between Pericytes and Infiltrating Monocytes/Macrophages after Spinal Cord Injury. *Am. J. Pathol.* **2017**, *187*, 639–653. [[CrossRef](#)]
70. Anenden, H. Burns. 2019. Available online: <https://www.who.int/news-room/fact-sheets/detail/burns> (accessed on 6 March 2018).
71. Sakallioğlu, A.E.; Basaran, O.; Karakayali, H.; Ozdemir, B.H.; Yucel, M.; Arat, Z.; Haberal, M. Interactions of systemic immune response and local wound healing in different burn depths: An experimental study on rats. *J. Burn. Care Res.* **2006**, *27*, 357–366. [[CrossRef](#)]
72. Horowitz, J.C.; Cui, Z.; Moore, T.A.; Meier, T.R.; Reddy, R.C.; Toews, G.B.; Standiford, T.J.; Thannickal, V.J. Constitutive activation of prosurvival signaling in alveolar mesenchymal cells isolated from patients with nonresolving acute respiratory distress syndrome. *Am. J. Physiol. Lung Cell Mol. Physiol.* **2006**, *290*, L415–L425. [[CrossRef](#)]
73. Choi, S.S.; Omenetti, A.; Witck, R.P.; Moylan, C.A.; Syn, W.K.; Jung, Y.; Yang, L.; Sudan, D.L.; Sicklick, J.K.; Michelotti, G.A.; et al. Hedgehog pathway activation and epithelial-to-mesenchymal transitions during myofibroblastic transformation of rat hepatic cells in culture and cirrhosis. *Am. J. Physiol. Gastrointest. Liver Physiol.* **2009**, *297*, G1093–G1106. [[CrossRef](#)] [[PubMed](#)]
74. Kolb, M.; Margetts, P.J.; Anthony, D.C.; Pitossi, F.; Gauldie, J. Transient expression of IL-1beta induces acute lung injury and chronic repair leading to pulmonary fibrosis. *J. Clin. Investig.* **2001**, *107*, 1529–1536. [[CrossRef](#)] [[PubMed](#)]
75. Chaudhuri, V.; Zhou, L.; Karasek, M. Inflammatory cytokines induce the transformation of human dermal microvascular endothelial cells into myofibroblasts: A potential role in skin fibrogenesis. *J. Cutan. Pathol.* **2007**, *34*, 146–153. [[CrossRef](#)] [[PubMed](#)]
76. Leaf, I.A.; Nakagawa, S.; Johnson, B.G.; Cha, J.J.; Mittelsteadt, K.; Guckian, K.M.; Gomes, I.G.; Altemeier, W.A.; Duffield, J.S. Pericyte MyD88 and IRAK4 control inflammatory and fibrotic responses to tissue injury. *J. Clin. Investig.* **2017**, *127*, 321–334. [[CrossRef](#)] [[PubMed](#)]
77. Wu, C.F.; Chiang, W.C.; Lai, C.F.; Chang, F.C.; Chen, Y.T.; Chou, Y.H.; Wu, T.H.; Linn, G.R.; Ling, H.; Wu, K.D.; et al. Transforming growth factor beta-1 stimulates profibrotic epithelial signaling to activate pericyte-myofibroblast transition in obstructive kidney fibrosis. *Am. J. Pathol.* **2013**, *182*, 118–131. [[CrossRef](#)] [[PubMed](#)]
78. Zannini, M.; Avantiaggiato, V.; Biffali, E.; Arnone, M.I.; Sato, K.; Pischetola, M.; Taylor, B.A.; Phillips, S.J.; Simeone, A.; Di Lauro, R. TTF-2, a new forkhead protein, shows a temporal expression in the developing thyroid which is consistent with a role in controlling the onset of differentiation. *EMBO J.* **1997**, *16*, 3185–3197. [[CrossRef](#)] [[PubMed](#)]
79. Golson, M.L.; Kaestner, K.H. Fox transcription factors: From development to disease. *Development* **2016**, *143*, 4558–4570. [[CrossRef](#)]
80. Rajendran, N.K.; Dhillip Kumar, S.S.; Houreld, N.N.; Abrahamse, H. Understanding the perspectives of forkhead transcription factors in delayed wound healing. *J. Cell Commun. Signal.* **2019**, *13*, 151–162. [[CrossRef](#)]
81. De Felice, M.; Di Lauro, R. Thyroid development and its disorders: Genetics and molecular mechanisms. *Endocr. Rev.* **2004**, *25*, 722–746. [[CrossRef](#)]
82. Aza-Blanc, P.; Di Lauro, R.; Santisteban, P. Identification of a cis-regulatory element and a thyroid-specific nuclear factor mediating the hormonal regulation of rat thyroid peroxidase promoter activity. *Mol. Endocrinol.* **1993**, *7*, 1297–1306.
83. Perrone, L.; Pasca Di Magliano, M.; Zannini, M.; Di Lauro, R. The thyroid transcription factor 2 (TTF-2) is a promoter-specific DNA-binding independent transcriptional repressor. *Biochem. Biophys. Res. Commun.* **2000**, *275*, 203–208. [[CrossRef](#)] [[PubMed](#)]
84. Santisteban, P.; Acebron, A.; Polycarpou-Schwarz, M.; Di Lauro, R. Insulin and insulin-like growth factor I regulate a thyroid-specific nuclear protein that binds to the thyroglobulin promoter. *Mol. Endocrinol.* **1992**, *6*, 1310–1317. [[PubMed](#)]

85. Fernandez, L.P.; Lopez-Marquez, A.; Martinez, A.M.; Gomes-Lopez, G.; Santisteban, P. New insights into FoxE1 functions: Identification of direct FoxE1 targets in thyroid cells. *PLoS ONE* **2013**, *8*, e62849. [[CrossRef](#)] [[PubMed](#)]
86. Wang, L.W.; Nandadasa, S.; Annis, D.S.; Dubail, J.; Mosher, D.F.; Willard, B.B.; Apte, S.S. A disintegrin-like and metalloproteinase domain with thrombospondin type 1 motif 9 (ADAMTS9) regulates fibronectin fibrillogenesis and turnover. *J. Biol. Chem.* **2019**, *294*, 9924–9936. [[CrossRef](#)]
87. Garrett, S.C.; Varney, K.M.; Weber, D.J.; Bresnick, A.R. S100A4, a mediator of metastasis. *J. Biol. Chem.* **2006**, *281*, 677–680. [[CrossRef](#)]
88. Hamilton, D.W. Functional role of periostin in development and wound repair: Implications for connective tissue disease. *J. Cell Commun. Signal.* **2008**, *2*, 9–17. [[CrossRef](#)]
89. Zhou, H.M.; Wang, J.; Elliot, C.; Wen, W.; Hamilton, D.W.; Conway, S.J. Spatiotemporal expression of periostin during skin development and incisional wound healing: Lessons for human fibrotic scar formation. *J. Cell Commun. Signal.* **2010**, *4*, 99–107. [[CrossRef](#)]
90. Yamaguchi, Y.; Ono, J.; Masuoka, M.; Ohta, S.; Izuhara, K.; Ikezawa, Z.; Aihara, M.; Takahashi, K. Serum periostin levels are correlated with progressive skin sclerosis in patients with systemic sclerosis. *Br. J. Dermatol.* **2013**, *168*, 717–725. [[CrossRef](#)]
91. Masuoka, M.; Shiraiishi, H.; Ohta, S.; Suzuki, S.; Arima, K.; Aoki, S.; Toda, S.; Inagaki, N.; Kurihara, Y.; Hayashida, S.; et al. Periostin promotes chronic allergic inflammation in response to Th2 cytokines. *J. Clin. Investig.* **2012**, *122*, 2590–2600. [[CrossRef](#)]
92. Matsuzawa, M.; Arai, D.; Nomura, Y.; Murata, T.; Yamakoshi, Y.; Oida, S.; Hanada, N.; Nakamura, Y. Periostin of human periodontal ligament fibroblasts promotes migration of human mesenchymal stem cell through the alphavbeta3 integrin/FAK/PI3K/Akt pathway. *J. Periodontal. Res.* **2015**, *50*, 855–863. [[CrossRef](#)]
93. Mael-Ainin, M.; Abed, A.; Conway, S.J.; Dussaule, J.C.; Chatziantoniou, C. Inhibition of periostin expression protects against the development of renal inflammation and fibrosis. *J. Am. Soc. Nephrol.* **2014**, *25*, 1724–1736. [[CrossRef](#)] [[PubMed](#)]
94. Cherubino, M.; Rubin, J.P.; Milijkovic, N.; Kelmendi-Doko, A.; Marra, K.G. Adipose-derived stem cells for wound healing applications. *Ann. Plast. Surg.* **2011**, *66*, 210–215. [[CrossRef](#)] [[PubMed](#)]
95. Mills, S.J.; Zhuang, L.; Arandjelovic, P.; Cowin, A.J.; Kaur, P. Effects of human pericytes in a murine excision model of wound healing. *Exp. Dermatol.* **2015**, *24*, 881–882. [[CrossRef](#)] [[PubMed](#)]
96. Rodriguez, J.; Boucher, F.; Lequeux, C.; Josset-Lamaugarny, A.; Rouyer, O.; Ardisson, O.; Rutschi, H.; Sigaudou-Roussel, D.; Damour, O.; Mojallal, A. Intradermal injection of human adipose-derived stem cells accelerates skin wound healing in nude mice. *Stem Cell Res. Ther.* **2015**, *6*, 241. [[CrossRef](#)] [[PubMed](#)]
97. Ji, G.H.; Cui, Y.; Yu, H.; Cui, X.B. Profiling analysis of FOX gene family members identified FOXE1 as potential regulator of NSCLC development. *Cell Mol. Biol.* **2016**, *62*, 57–62.
98. Lammer, E.J.; Mohammed, N.; Iovannisci, D.M.; Ma, C.; Lidral, A.C.; Shaw, G.M. Genetic variation of FOXE1 and risk for orofacial clefts in a California population. *Am. J. Med. Genet. A* **2016**, *170*, 2770–2776. [[CrossRef](#)]
99. Dai, W.; Meng, X.; Mo, S.; Xiang, W.; Xu, Y.; Zhang, L.; Wang, R.; Li, Q.; Cai, G. FOXE1 represses cell proliferation and Warburg effect by inhibiting HK2 in colorectal cancer. *Cell Commun. Signal.* **2020**, *18*, 13. [[CrossRef](#)]
100. Shao, X.; Wei, X. FOXP1 enhances fibrosis via activating Wnt/beta-catenin signaling pathway in endometriosis. *Am. J. Transl. Res.* **2018**, *10*, 3610–3618.
101. Vivar, R.; Humeres, C.; Munoz, C.; Boza, P.; Bolivar, S.; Tapia, F.; Lavandero, S.; Chiong, M.; Diaz-Araya, G. FoxO1 mediates TGF-beta1-dependent cardiac myofibroblast differentiation. *Biochim. Biophys. Acta* **2016**, *1863*, 128–138. [[CrossRef](#)]
102. Mori, R.; Tanaka, K.; de Kerckhove, M.; Okamoto, M.; Kashiwayama, K.; Tanaka, K.; Kim, S.; Kawata, T.; Komatsu, T.; Park, S.; et al. Reduced FOXO1 expression accelerates skin wound healing and attenuates scarring. *Am. J. Pathol.* **2014**, *184*, 2465–2479. [[CrossRef](#)]

